Vol. 8
Issue 2
2019

ASSAYWISE LETTER

LIFE SCIENCE RESOURCES AND APPLICATIONS

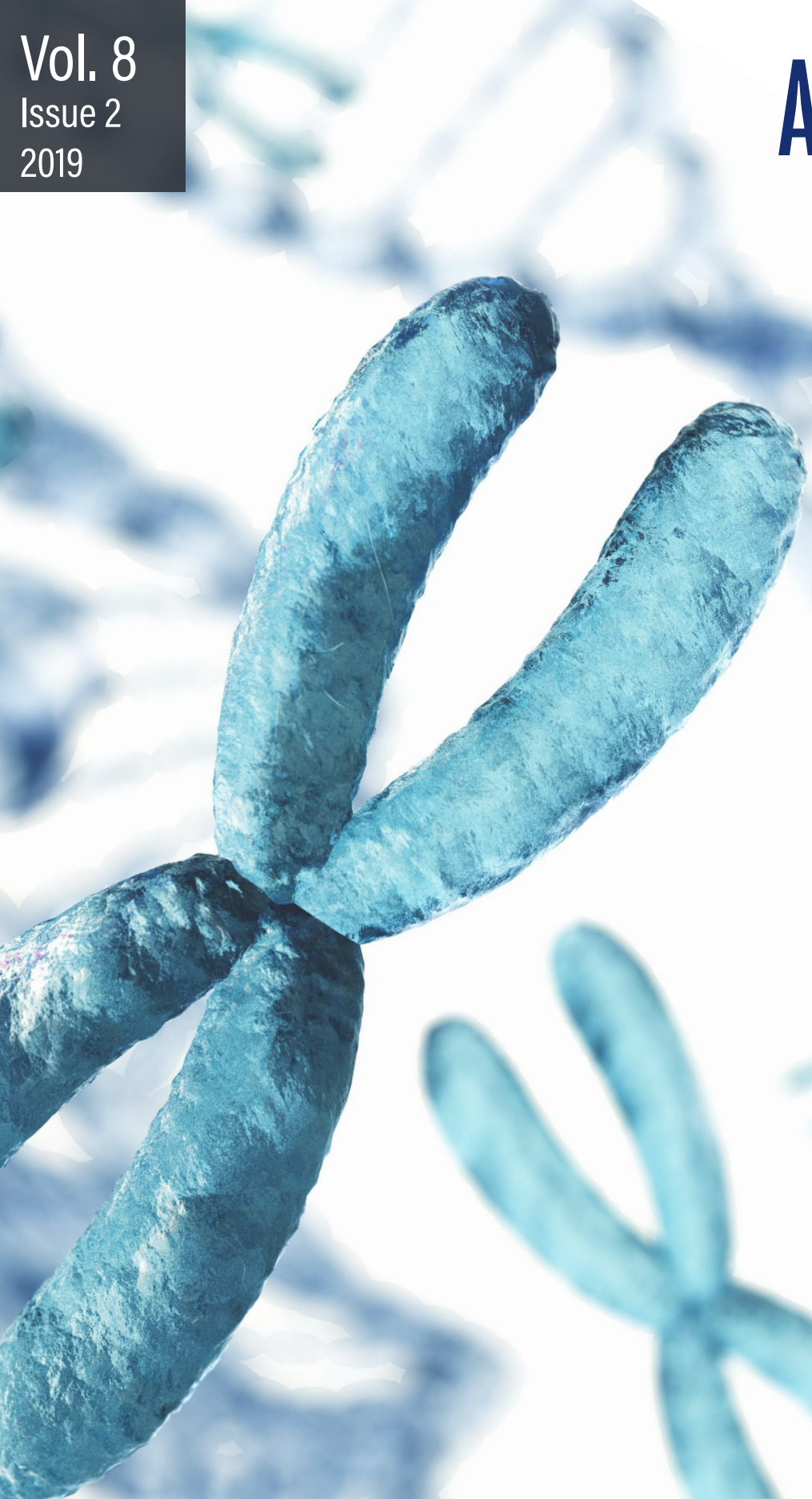

Featuring

AAT Bioquest®

TABLE OF CONTENTS

AAT Bioquest®

A Simple End-Point Calcium Assay

Using a Green Fluorescent Indicator Fluo-8E™, AM

Abstract

The intracellular release of calcium from internal stores upon GPCR stimulation is transient. To study this transient calcium signaling in a microplate format, a fluorescence plate reader that has a built-in liquid handling system and kinetic reading capability is often required. This limits the usage of the conventional fluorescence plate readers to conduct studies on calcium signaling. We report the development of an endpoint calcium assay that can be used to monitor the effects of GPCR modulators in calcium response cell-based assays with conventional fluorescence microplate readers using bottom reading mode. Fluo-8E™ AM, a cell permeant, non-fluorescent calcium indicator that has enhanced and long-lived fluorescence upon calcium binding was used in this assay. We demonstrated the capability of this assay to accurately determine the EC50 of numbers of GPCR modulators. The results are comparable to the results from assays utilizing the widely used fluorescent calcium indicators Fluo-4 AM and Fluo-3 AM in kinetic assays.

Introduction

Calcium is a ubiquitous secondary messenger that controls a spectrum of cellular processes. Cells generate their calcium signals by utilizing both internal and external sources of calcium. The internal storage of calcium is located within the membrane of the endoplasmic reticulum (ER) and sarcoplasmic reticulum (SR). When stimuli bind to cell surface receptors (e.g. GPCR), calcium is released from the internal stores through various channels including InsP3R and members from the ryanodine receptors (RYRs) family [1][2]. The intracellular calcium concentration rises from 100 nM to roughly 1 μM as a result. After the calcium-induced signaling is completed, calcium is removed from the cytoplasm to restore the resting state [3].

Fluorescent calcium indicators have been widely used to monitor the calcium motility in in vitro, in vivo and ex vivo applications. The introduction of the first generation calcium fluorescent indicators (Indo-1, Fura-2, Fluo-3 and Rhod-2) in the 1980s made measuring calcium signaling using fluorescent instruments possible [4][5]. The second generation calcium indicator Fluo-4 has a much improved S/B ratio and is popularly used in high throughput screening, confocal imaging and flow cytometry [6]. However, in order to monitor the transient calcium flux inside cells using these calcium indicators in microplates, one has to use a fluorescence plate reader (e.g. FlexStation, FLIPR, FDSS) that has a built-in liquid handling system for adding the desired agonists/antagonists, and also the ability to read the signal changes in kinetic mode. This limits researchers who desire to use conventional fluorescence microplate readers to study the effects of GPCR modulators in calcium signaling.

We have developed an endpoint calcium assay allowing the use of conventional fluorescence microplate readers to accurately determine the EC_{50} of GPCR modulators. Fluo-8E™ AM is a fluorescent calcium indicator that has the same spectral properties as Fluo-3 AM and Fluo-4 AM (Ex/Em = 485 nm/525 nm). Fluo-8E™ AM can cross cell membrane passively by diffusion. Once inside the cells, the lipophilic blocking groups of Fluo-8E™ AM are cleaved by intracellular esterase, resulting in a negatively charged fluorescent dye that stays inside cells. Its fluorescence is enhanced by >100 times upon binding to

calcium and is sustained for 1-2 minutes with insignificant signal decrease (Figure 1). The Fluo-8E™ AM assay does not require the addition of any organic anion transporter inhibitors to prevent dye leakage from cells. It also does not need any wash steps to lower background signal and achieve high S/B ratio. These characteristics make Fluo-8E™ AM ideal for the measurement of cellular calcium response using conventional fluorescence microplate readers that do not have a built-in liquid handling system or kinetic reading capability. One can simply add the agonist/antagonist via an external liquid handler or a handheld pipettor, and detect the changes in fluorescence with a bottom read conventional fluorescence microplate reader.

In this technical report, we determined the EC_{50} of modulators of different GPCRs using the endpoint Fluo-8E™ AM assay via a conventional fluorescent microplate reader in a 96-well plate and 384-well plate format. The sensitivity and accuracy of the results using the endpoint Fluo-8E™ AM assay is comparable to the results from using the popular Fluo-3 AM and Fluo-4 AM kinetic assays.

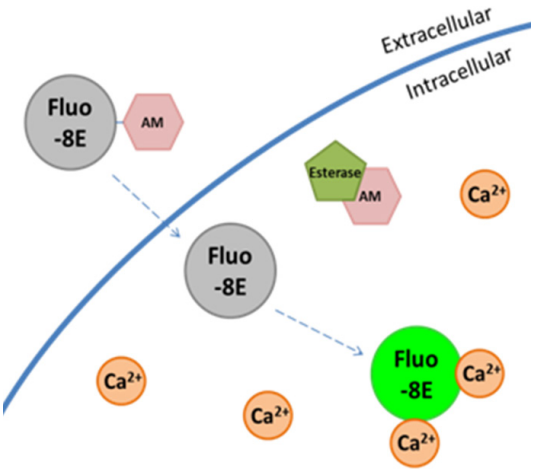

Figure 1. Fluo-8E™ AM Assay Principle. Fluorescent calcium indicator Fluo-8E™ AM can cross cell membrane passively by diffusion. Once inside the cells, the lipophilic blocking groups of Fluo-8E™ AM are cleaved by esterase, resulting in a negatively charged fluorescent dye that stays inside cells. Its fluorescence is enhanced by >100 times upon binding to calcium.

Materials and Methods

Cell Culture

Cell lines were purchased from ATCC (Manassas, VA). CHO-K1 cells were maintained in F-12K medium with 10% FBS and 1% Penicillin-Streptomycin-Glutamine (Thermo Fisher, Waltham, MA). CHO-M1 cells were CHO-K1 cells stably transfected with rat M1 muscarinic acetylcholine receptor. CHO-M1 cells were maintained in F-12K medium with 10% FBS, 1% Penicillin-Streptomycin-Glutamine and 250 µg/mL G-418 (Thermo Fisher, Waltham, MA). HEK-293 cells were maintained in DMEM with 10% FBS and 1% Penicillin-Streptomycin-glutamine (Thermo Fisher, Waltham, MA).

Reagent Preparation

10 µg/mL Fluo-8E™ AM (AAT Bioquest Sunnyvale, CA) was diluted in 1X assay buffer. 10 µg/mL Fluo-3 AM and Fluo-4 AM (AAT Bioquest, Sunnyvale, CA) were prepared in HHBS (AAT Bioquest, Sunnyvale, CA) containing 0.04% Pluronic F127 (AAT Bioquest, Sunnyvale, CA) with or without 5 mM probenecid (AAT Bioquest, Sunnyvale, CA). ATP and carbachol titrations (Sigma, St Louis, MO) were prepared in Hanks and 20 mM Hepes buffer (HHBS).

Calcium Kinetic and Endpoint Assays

Cells were plated in 100 µL/25 µL culture medium in 96-well/384-wellclear bottom black plates (Greiner Bio-One, Kremsmunster, Austria) at 50,000/12,500 cells per well. The next day, equal volume of prepared dye-loading solutions that contain calcium indicators were added to each well. The cells were incubated with the dye-loading buffer for 60 min at 37 °C, 5% CO_2 incubator. When cells were incubated with the Fluo-8E™ AM, probenecid was not needed and the cells were not washed following the incubation. On the other hand, probenecid and wash steps were required when using Fluo-3 AM and Fluo-4 AM to prevent the leakage of the indicators and to lower the background signal. The calcium kinetic assays were performed on FlexStation® (Molecular Devices, Sunnyvale, CA) using the built-in liquid handler to add the calcium flux stimulants and the kinetic reading mode to capture the changes in fluorescence signal over time. The endpoint assays were conducted by adding the stimulants with handheld multichannel pipettors immediately followed by the detection of the fluorescence using bottom read mode on ClarioStar® fluorescence microplate reader (BMG Labtech, Cary, NC).

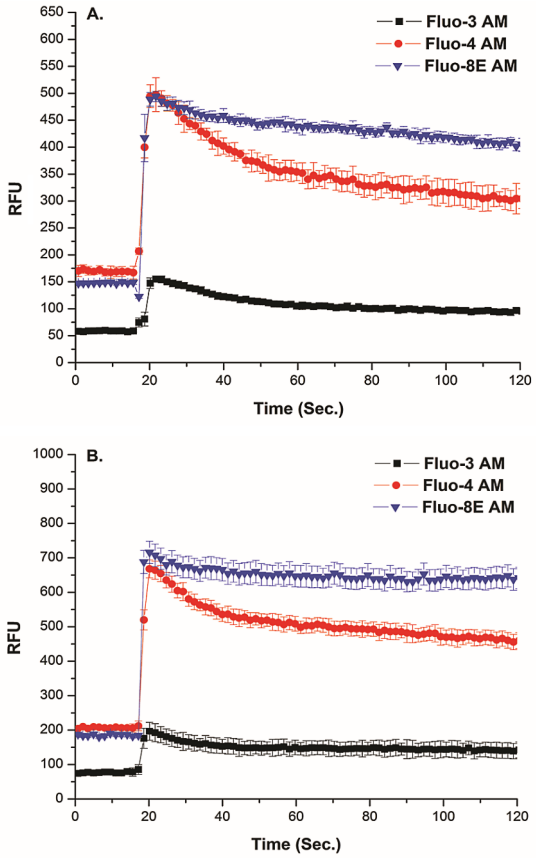

Figure 2. The measurement of calcium response upon ATP and carbachol stimulation in CHO-K1 and CHO-M1 cells, respectively. CHO-K1 (A) or CHO-M1 (B) cells were incubated with 5 µg/mL of Fluo-3 AM, Fluo-4 AM or Fluo-8E™ AM for 60 min at 37°C. The cellular signal was monitored before and after the addition of ATP (A) or carbachol (B) by FlexStation® using kinetic reading mode for 120 seconds. Data shown are mean ± SEM of triplicate wells and are representative of three independent experiments. Black square indicates Fluo-3 AM incubated cells, red circle indicates Fluo-4 AM incubated cells and blue triangle indicates Fluo-8E™ AM incubated cells.

Data Analysis

The kinetic calcium assay data were simultaneously collected by SoftMax®Pro (Molecular Devices, Sunnyvale, CA). The dose dependent calcium response data were analyzed on Origin (OriginLab Corporation, Northampton, MA). The dose response curve is generated and defined by the four parameters: the baseline response (Bottom), the maximum response (Top), the slope (Hill slope), and the drug concentration that provokes a response halfway between baseline and maximum (EC_{50}). Error bars were calculated using standard error of the mean (S.E.M.). The statistical significance ($p<0.05$) was calculated using student's t-test from triplicates wells in three independent experiments. The Z factor ($1> Z > 0.5$)calculation was used for data quality assessment of assay conditions (10).

Results and Discussion

ATP and Carbochol Induced Calcium Response in CHO-K1 and CHO-M1 Cells using FLuo-8E™ AM

In order to capture the fluorescent signal induced by the transient calcium movement inside the cells upon stimulation without using the kinetic reading mode, a calcium assay that has a long-lived signal is needed. We measured the calcium kinetic signal of ATP stimulated endogenous P2Y receptors in CHO-K1 cells and carbachol stimulated rat M1 muscarinic acetylcholine receptors in CHO-M1 cells using Fluo-8E™ AM, and observed a long-lived signal upon stimulation.

In order to observe the signal of calcium flux in CHO-K1 and CHO-M1 cells, 10 µM ATP or 1 µM of carbachol, respectively, were added using FlexStation® built-in liquid handler and the calcium flux was monitored for 120 seconds. The S/B_{max} was calculated by dividing the peak signal after ATP or carbachol addition and the basal signal before ATP or carbachol addition. In ATP stimulation assay, The Fluo-8E™ AM produced similar high S/B_{max} ratio (4 fold) as Fluo-4 AM (4 fold), and much higher overall signal and S/B_{max} ratio than Fluo-3 AM (2 fold) (Figure 2A). More interestingly, the Fluo-8E™ AM showed much slower signal decay (Figure 2A) than Fluo-3 AM and Fluo-4 AM. The signal reduction after ATP addition at 30, 60 and 90 seconds was compared between the three dye-loading methods. When using the Fluo-8E™ AM, the signal reduced only 10% after 30 seconds, 13.6% after 60 seconds and 16.9% after 90 seconds, which is twice slower compare to that using Fluo-3 AM and Fluo-4 AM. Fluo-3 AM and Fluo- 4 AM reduced 28.4% and 27.3% after 30 seconds, 35.2% and 34.5% after 60 seconds and 37.6% and 38.5% after 90 seconds, respectively.

In carbachol stimulation assay, the signal generated by using Fluo-8E™ AM showed the slowest signal decrease after the addition of carbachol among the three dye-loading methods (Figure 2B). When using the Fluo-8E™ AM, the signal reduced only 9% after 30 seconds, 9.2% after 60 seconds and 10.6% after 90 seconds, which is more than 2 times slower than

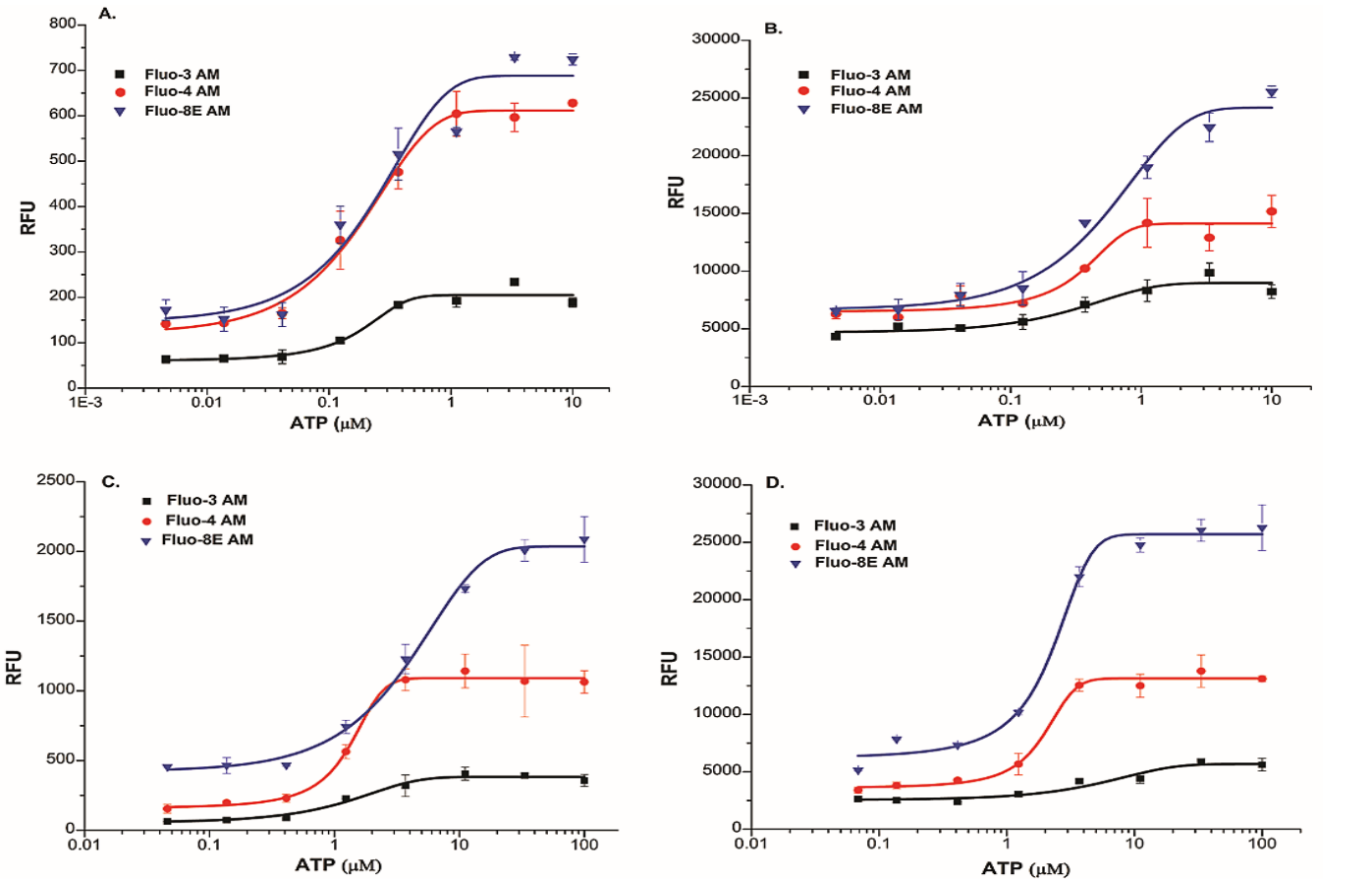

Figure 3. The ATP dose dependent calcium flux in CHO-K1 and HEK 293 cells. CHO-K1 cells or HEK 293 cells were incubated with 5 μg/mL of Fluo-3 AM, Fluo-4 AM or Fluo-8E AM for 60 min at 37°C. Upon addition of different concentrations of ATP, the cellular signal was monitored by FlexStation® using kinetic reading mode (A: CHO-K1, C: HEK 293) for 120 seconds or by ClarioStar® using endpoint reading mode (B: CHO-K1, D: HEK 293). Data shown are mean ± SEM of triplicate wells and are representative of three independent experiments. Black square indicates Fluo-3 AM incubated cells, red circle indicates Fluo-4 AM incubated cells and blue triangle indicates Fluo-8E™ AM incubated cells.

that using Fluo-3 AM and Fluo-4 AM. Fluo-3 AM and Fluo-4 AM reduced 25% and 22.5% after 30 seconds, 25.7% and 26.4% after 60 seconds and 27.7% and 30.4% after 90 seconds, respectively. These observations are consistent with the results obtained from ATP stimulation assays in CHO-K1 cells and indicate the potential application of Fluo-8E™ AM to capture calcium movement in measuring GPCR activity like endogenous P2Y receptors and exogenous M1 receptors using endpoint reading mode.

The ATP Dose Dependent Inducton of Calcium Flux in CHO-K1 and HEK 239 Cells Using Kinetic and Endpoint Assays

We evaluated the S/B ratio and EC_{50} of ATP in CHO-K1 and HEK 293 cells using Fluo-8E™ AM in both kinetic and endpoint assays. The S/B_{max} ratio was calculated using the signals from the CHO-K1 cells and HEK 293 cells added with the highest concentration of ATP and the cells with no ATP addition. EC_{50} of ATP was determined by plotting the signal changes at different concentrations of ATP in CHO-K1 cells and HEK 293 cells.

In CHO-K1 cells with kinetic assay, the Fluo-8E™ AM showed similar S/B ratio (4.4 fold) as Fluo-4 AM (4.3 fold), and much higher overall signal and S/B ratio than that of Fluo-3 AM (2 fold). The similar EC_{50} (~ 0.2 μM, Table 1) was observed in all three assays with different dye-loading methods (Figure 3A), and the EC_{50} is in line with previously published values [7]. However, with endpoint reading mode, the S/B ratio is significantly decreased in the assays using Fluo-3 AM (1.5 fold, $p<0.05$) and Fluo-4 AM (2.4 fold, $p<0.05$), when compared to kinetic assay. On the other

hand, S/B ratio only slightly deceased in the assay using Fluo-8E™ AM (3.9 fold). This can be explained by the faster signal decay in Fluo-3 AM and Fluo-4 AM assays than that of Fluo-8E™ AM assay upon ATP stimulation (Figure 2A). The EC_{50} of ATP in endpoint assays was slightly higher than kinetic assays in all three methods (Figure 3B, Table 1).

In HEK 293 cells with kinetic assay, the Fluo-8E™ AM showed similar S/B ratio (4.5 fold) as Fluo-4 AM (5.4 fold) and Fluo-3 AM (5.8 fold). The similar EC_{50} (Table 2) was observed in all three assays with different dye-loading methods (Figure 3C), and the EC_{50} is in line with previously published values [7]. When using endpoint reading mode, however, the S/B ratio is significantly decreased in the assays using Fluo-3 AM (2.1 fold, $p<0.05$) and Fluo-4 AM (3.8 fold, $p<0.05$), when compared to kinetic assay. On the other hand, S/B ratio only slightly deceased in the assay using Fluo-8E™ AM (5 fold). The EC_{50} of ATP in endpoint assays was comparable to kinetic assays in Fluo-8E™ AM and Fluo-4 AM assays (Figure 3D, Table 2).

This demonstrates that Fluo-8E™ AM produced similar results as Fluo-4 AM and Fluo-3 AM in kinetic reading, and is more suitable than Fluo-3 AM and Fluo-4 AM assay to conduct the calcium mobility assay using endpoint reading mode with insignificant signal and EC_{50} changes.

The Carbachol Dose Dependent Calcium Response in CHO-M1 Cell Using Kinetic and Endpoint Assays

When using the Fluo-8E AM to measure the S/B_{max} and the EC_{50} of carbachol using kinetic and endpoint assays, the S/B_{max} ratios are 3.8 fold and 3.9 fold respectively, and the EC_{50} of carbachol were determined to be 0.13 μM and 0.14 μM, respectively (Figure 4A and B, Table 3). Although the EC_{50} did not show significant changes between kinetic reading

Table 1. ATP dose dependent calcium flux in CHO-K1 cells.

	Fluo-3 AM	Fluo-4 AM	Fluo-8E™ AM
Kinetic Reading			
S/B	2	4.4	4.3
***EC_{50} (μM)**	0.18 ± 0.025	0.18 ± 0.027	0.2 ± 0.019
Endpoint Reading			
S/B	1.5^{s}	2.4^{s}	3.9^{ns}
***EC_{50} (μM)**	0.32 ± 0.031	0.38 ± 0.047	0.59 ± 0.039

*EC_{50} = mean ± s.e.m., n=3
^{s} = $p < 0.05$
^{ns} = No significant difference compared to kinetic assay

Table 2. ATP dose dependent calcium flux in HEK 293 cells.

	Fluo-3 AM	Fluo-4 AM	Fluo-8E™ AM
Kinetic Reading			
Signal/Background	5.8	5.4	4.5
***EC_{50} (μM)**	1.29 ± 0.37	1.36 ± 0.21	2.5 ± 0.27
Endpoint Reading			
Signal/Background	2.1^{s}	2.4^{s}	5.0^{ns}
***EC_{50} (μM)**	0.32 ± 0.031	0.38 ± 0.047	0.59 ± 0.039

*EC_{50} = mean ± s.e.m., n=3
^{s} = $p < 0.05$
^{ns} = No significant difference compared to kinetic assay

mode and endpoint reading mode in Fluo-3 AM and Fluo-4 AM incubated cells , the S/B_{max} ratio decreased significantly in both assays (Figure 4A and B, Table 3, $p<0.05$). These results demonstrate that the Fluo-8E™ AM is suitable to determine the calcium response and EC_{50} of carbachol in CHO-M1 cells using conventional fluorescence microplate readers with the endpoint reading.

The Atropine Dose Dependent Inhibition of Calcium Flux in CHO-M1 Cell Using Kinetic and Endpoint Assays

To test the Fluo-8E™ AM in an antagonist assay, the dose dependent inhibition of atropine in muscarinic M1 receptor induced calcium response was performed in CHO-M1 cells. The dye loading was performed using Fluo-8E™ AM, Fluo-3 AM or Fluo-4 AM. Different concentrations of atropine were incubated with the cells for additional 15 min. The calcium response in CHO-M1 cells was captured either by kinetic assay before and after the addition of 1 μM carbachol using FlexStation®, or by endpoint reading after the addition of 1 μM carbachol using ClarioStar®. When using the Fluo-8E™ AM to measure the S/B and the EC_{50} of atropine using kinetic and endpoint assays, the S/B ratios are 3.5 fold and 3.14 fold respectively, and the calculated EC_{50} of atropine are 1.2 ± 0.2 nM and 0.8 ± 0.09 nM, respectively (Figure 5A and B, Table 4). Although the EC_{50} did not show significant changes between kinetic reading mode and endpoint reading mode in Fluo-3 AM and Fluo-4 AM incubated cells , Fluo-3 AM showed weak signal and low S/B, and the S/B ratio decreased significantly in Fluo-4 AM assay (Figure 5A

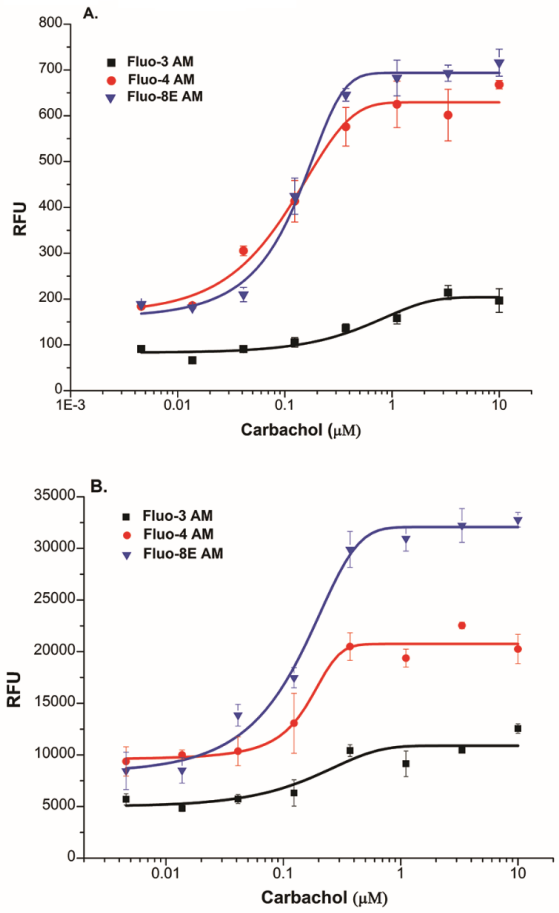

Fig. 4. The carbachol dose dependent calcium flux in CHO-M1cells. CHO-M1 cells were incubated with 5 μg/mL of Fluo-3 AM, Fluo-4 AM or Fluo-8E AM for 60 min at 37°C. The cellular signal was monitored before and after the addition of different concentrations of carbachol by FlexStation using kinetic reading mode (A) for 120 seconds or by ClarioStar using endpoint reading mode (B). Data shown are mean ± SEM of triplicate wells and are representative of three independent experiments. Black square indicates Fluo-3 AM incubated cells, red circle indicates Fluo-4 AM incubated cells and blue triangle indicates Fluo-8E AM incubated cells.

Table 3. Carbachol dose dependent calcium flux in CHO-M1 Cells.

	Fluo-3 AM	Fluo-4 AM	Fluo-8E™ AM
Kinetic Reading			
Signal/Background	2.6	3.7	3.8
***EC_{50} (μM)**	0.53 ± 0.005	0.1 ± 0.018	0.13 ± 0.022
Endpoint Reading			
Signal/Background	2^{s}	2.2^{s}	3.9^{ns}
***EC_{50} (μM)**	0.38 ± 0.030	0.12 ± 0.087	0.14 ± 0.02

*EC_{50} = mean ± s.e.m., n=3
^{s} = $p < 0.05$
^{ns} = No significant difference compared to kinetic assay

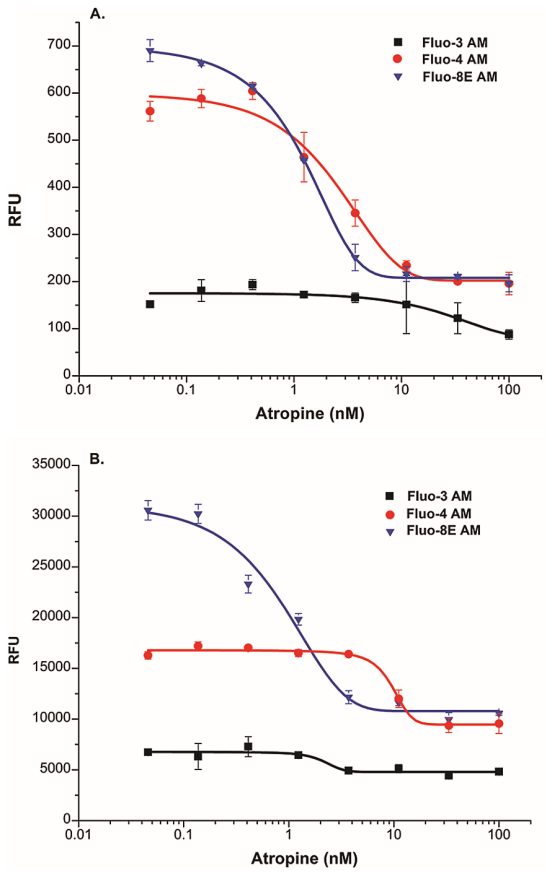

Figure 5. The atropine dose dependent inhibition of calcium flux in CHO-M1 cells. CHO-M1 cells were incubated with 5 µg/mL of Fluo-3 AM, Fluo-4 AM or Fluo-8E™ AM for 60 min at 37°C. Different concentration of Atropine was added to the cells and incubated for additional 15 min. The cellular signal was monitored before and after the addition of carbachol by FlexStation® using kinetic reading mode (A) for 120 seconds or by ClarioStar® using endpoint reading mode (B). Data shown are mean ± SEM of triplicate wells and are representative of three independent experiments. Black square indicates Fluo-3 AM incubated cells, red circle indicates Fluo-4 AM incubated cells and blue triangle indicates Fluo-8E™ AM incubated cells.

and B, Table 4, $p<0.05$). The results showed that the Fluo-8E™ AM is capable to determine the calcium response and EC_{50} of antagonist in CHO-M1 cells using fluorescence microplate readers in endpoint reading mode.

The Probenecid Free Calcium Assay in CHO-K1 Cells Using Fluo-8E™ AM

Cell types like CHO and HeLa have high organic anion transporters activity, fluorescent calcium indicators are poorly retained in those cell lines without the presence of the organic anion transporter inhibitor such as probenecid [7]. In standard calcium assay protocols using Fluo-3 AM or Fluo-4 AM, probenecid is required in the assay to achieve the optimal cellular retention.

The organic anion transporter inhibitors are toxic to cells and some of them are known to be the inhibitors of certain GPCRs (e.g. chemokine receptors, bitter taste receptors) [8] [9]. Fluo-8E™ AM has good cell retention and keeps the dye inside the cells without using probenecid. To assess the performance in calcium assays without probenecid, CHO-K1 cells were incubated with Fluo-3 AM, Fluo-4 AM and Fluo-8E™ AM dye-loading solutions without probenecid. 10 µM of ATP was transferred using FlexStation and kinetic read was used. The data showed that without probenecid, Fluo-3 AM and Fluo-4 AM showed poor response upon ATP stimulation, however, Fluo-8E™ AM still had good calcium response with S/B = 4 and EC_{50} of ATP at 0.2 ± 0.034 µM (Figure 6). Using the endpoint reading mode with ClarioStar® fluorescence microplate reader, similar results were observed (data not shown).

Table 4. Atropine dose dependent calcium flux in CHO-M1 cells.

	Fluo-3 AM	Fluo-4 AM	Fluo-8E™ AM
Kinetic Reading			
Signal/Background	2.2	3.5	3.5
***EC_{50} (µM)**	3.6 ± 0.8	2.5 ± 0.65	1.2 ± 0.2
Endpoint Reading			
Signal/Background	1.9^{ns}	1.99^{s}	3.14^{ns}
***EC_{50} (µM)**	4 ± 0.35	8.4 ± 0.52	0.8 ± 0.09

*EC_{50} = mean ± s.e.m., n=3
^{s} = $p < 0.05$
^{ns} = No significant difference compared to kinetic assay

Z factor Determination in 96-well Plate and Assay Miniaturization

The Z factor was determined in 96-well and 384-well plate format. In a 96-well plate assay, the layout of the plate and the summary of the Z factor were summarized in Table 5 and Table 6. The Z factor was calculated by using the formulation [10]:

$$Z = 1 - \frac{3(SD_{max} + SD_{min})}{AVG_{max} - AVG_{min}}$$

SD_{max} is standard deviation of maximal signal controls. SDmin is standard deviation of minimal signal controls. AVG_{max} is the mean value of maximal signal controls. AVG_{min} is the mean value of minimal signal controls.

The results showed that using Fluo-8E™ AM in an endpoint assay the Z factor is 0.64 which is better than the resultsthat using Fluo-3 AM (Z = 0.1) and Fluo-4 AM (Z = 0.45). As 1 ≥ Z ≥ 0.5 is required to be a suitable assay for screening purpose [10], only Fluo-8E™ AM is appropriate to use in an endpoint assay. The endpoint assay is appropriate to read for a whole 96-well plate immediately after the addition of calcium flux stimulant.

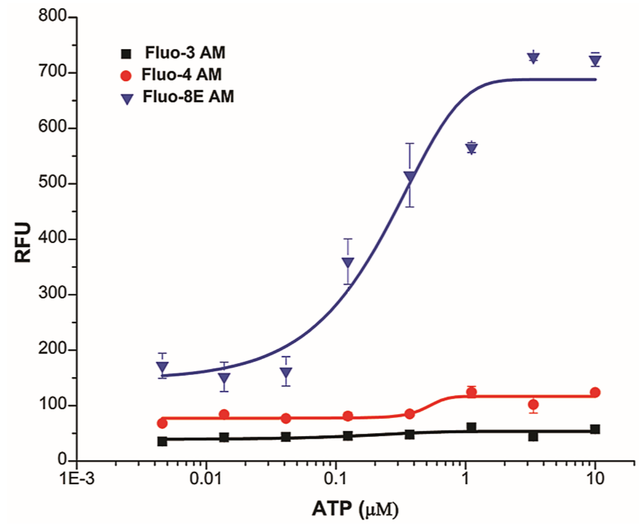

Figure 6. The ATP dose dependent calcium flux in CHO-K1 cells in a probenecid free assay. CHO-K1 cells were incubated with 5 µg/mL of Fluo-3 AM, Fluo-4 AM without probenecid or Fluo-8E™ AM for 60 min at 37°C. The cellular signal was monitored by FlexStation® before and after the addition of different concentrations of ATP using kinetic reading mode for 120 seconds. Data shown are mean ± SEM of triplicate wells and are representative of three independent experiments. Black square indicates Fluo-3 AM incubated cells, red circle indicates Fluo-4 AM incubated cells and blue triangle indicates Fluo-8E™ AM incubated cells.

Table 5. Plate layout for Z factor testing in CHO-K1 cells with or without ATP treatment in 96-well plate.

96-well plate											
Max.	Min.	Max.	Min.	Max.	Min.	Max.	Min.	Max.	Min.	Max.	Min.
Max.	Min.	Max.	Min.	Max.	Min.	Max.	Min.	Max.	Min.	Max.	Min.
Max.	Min.	Max.	Min.	Max.	Min.	Max.	Min.	Max.	Min.	Max.	Min.
Max.	Min.	Max.	Min.	Max.	Min.	Max.	Min.	Max.	Min.	Max.	Min.
Max.	Min.	Max.	Min.	Max.	Min.	Max.	Min.	Max.	Min.	Max.	Min.
Max.	Min.	Max.	Min.	Max.	Min.	Max.	Min.	Max.	Min.	Max.	Min.
Max.	Min.	Max.	Min.	Max.	Min.	Max.	Min.	Max.	Min.	Max.	Min.

Table 6. Z factor testing of calcium response in CHO-K1 cells in endpoint assay in 96-well plate.

	Fluo-3 AM	Fluo-4 AM	Fluo-8E™ AM
AVG_{max}	9702.1	21188.6	25330.3
CV_{max}	7.3	7.9	4.8
AVG_{min}	6006.3	9702.1	7089.5
CV_{min}	6.9	4.5	4.9
Z Factor	0.1	0.5	0.64
S/B	1.6	2.2	3.6

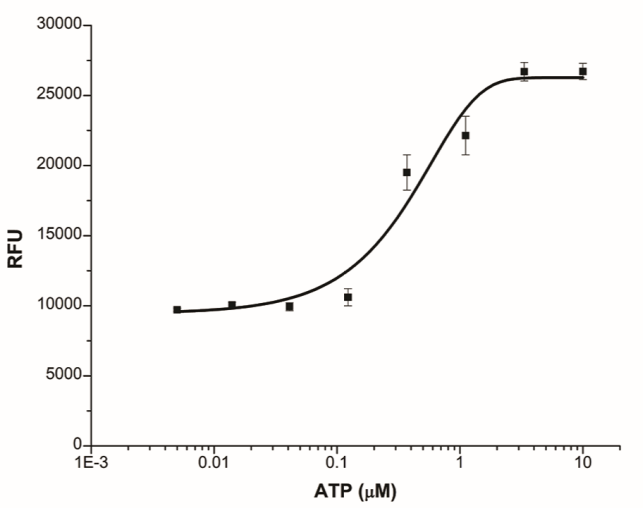

Figure 6. The ATP dose dependent calcium flux in CHO-K1 cells using a 384-well format. CHO-K1 cells were incubated with 5 μg/mL of Fluo-8E™ AM for 60 min at 37°C. Upon addition of different concentrations of ATP, the cellular signal was monitored by ClarioStar using endpoint reading mode. Data shown are mean ± SEM of 10 wells and are representative of three independent experiments.

The detailed protocol of 96-well plate assay is listed in Table 7.

The Fluo-8E™ AM endpoint assay can also be adapted into 384-well plate format (see Table 7 for detailed protocol). The calculated EC_{50} of ATP (0.61 ± 0.072 μM) in CHO-K1 cells is comparable to the results from 96-well plate (Figure 7).

Summary

The calcium probe Fluo-8E™ AM was tested in different cell lines using the kinetic and the endpoint assays. The two widely used fluorescent calcium indicators Fluo-3 AM and Fluo-4 AM are used as benchmarks. Using kinetic assay, Fluo-8E™ AM showed similar results as Fluo-3 AM and Fluo-4 AM. There are no differences in S/B ratio and EC_{50} of agonists and antagonists measured in kinetic assay and endpoint assay using Fluo-8E™ AM. In conclusion, this endpoint calcium assay provides an alternative to the existing kinetic calcium assay methods, which allows researchers to study calcium flux in endpoint reading with a conventional inexpensive fluorescence microplate reader with comparable results to the assay performed using the kinetic reading mode.

Table 7. Assay protocol table for 96-well/384-well plate.

Step	Parameter	96-well / 384-well	Description
1	Plate cells	100 µL / 25 µl	50,000 cells / 12,500 cells
2	Fluo-8E™, AM	100 µL / 25 µl	Add 2X Fluo-8E™, AM
3	Incubation time	1 hr	37°C, 5% CO_2
4	Optional - antagonist	10 µL / 2.5 µL	Add 20X of antagonist using a handheld pipettor or a liquid handler
5	Incubation time	15 min	37°C, 5% CO_2
6	Agonist	50 µL/ 25 µL	Add 5X (96-well) or 3X (384-well) of stimulant using a handheld pipettor or a liquid handler
7	Assay readout	Ex/Em = 490 nm/ 525 nm, Cutoff = 515 nm	Fluorescence microplate reader, bottom read, endpoint read mode

Step	Notes
1	96-well or 384-well tissue culture-treated black plates with clear bottom
2	Dissolve Fluo-8E, AM in DMSO and dilute in the 1X assay buffer (dilution factor 1: 500)
3	Incubate in the cell incubator with plate lid on
4	Transfer the antagonist (e.g. Atropine) using an 8-channel handheld pipettor or a liquid handler with 8-tip dispensing
5	Incubate in the cell incubator with plate lid on
6	Transfer the agonist (e.g. ATP, Carbachol) using an 8-channel handheld pipettor or a liquid handler with 8-tip dispensing
7	Read the plate on the fluorescence microplate reader as soon as the agonist is added

References

1. M. J. Berridge, "Inositol trisphosphate and calcium signalling," Nature, vol. 361, no. 6410, pp. 315–325, 1993.
2. D. E. Clapham, "Calcium Signaling," Cell, vol. 131, no. 6. pp. 1047–1058, 2007.
3. M. J. Berridge, P. Lipp, and M. D. Bootman, "The versatility and universality of calcium signalling.," Nat. Rev. Mol. Cell Biol., vol. 1, no. 1, pp. 11–21, 2000.
4. R. Y. Tsien, "New Calcium Indicators and Buffers with High Selectivity Against Magnesium and Protons: Design, Synthesis, and Properties of Prototype Structures," Biochemistry, vol. 19, no. 11, pp. 2396–2404, 1980.
5. R. Y. Tsien, "A non-disruptive technique for loading calcium buffers and indicators into cells," Nature, vol. 290, no. 5806, pp. 527–528, 1981.
6. P. Coward, S. D. H. Chan, H. G. Wada, G. M. Humphries, and B. R. Conklin, "Chimeric G proteins allow a high-throughput signaling assay of G(i)- coupled receptors," Anal. Biochem., vol. 270, no. 2, pp. 242–248, 1999.
7. X. Li, I. Llorente, and M. Brasch, "Improvements in live cell analysis of G protein coupled receptors using second generation BD calcium assay kits.," Curr. Chem. Genomics, 2008.
8. A. Visegrády, A. Boros, Z. Némethy, B. Kiss, and G. M. Keseru, "Application of the BD ACTOne™ technology for the high-throughput screening of Gs-coupled receptor antagonists," J. Biomol. Screen., vol. 12, no. 8, pp. 1068–1073, 2007.
9. T. A. Greene, S. Alarcon, A. Thomas, E. Berdougo, B. J. Doranz, P. A. S. Breslin, and J. B. Rucker, "Probenecid inhibits the human bitter taste receptor TAS2R16 and suppresses bitter perception of salicin," PLoS One, vol. 6, no. 5, 2011.
10. J.-H. Zhang, T. D. Y. Chung, and K. R. Oldenburg, "A Simple Statistical Parameter for Use in Evaluation and Validation of High Throughput Screening Assays," J. Biomol. Screen., 1999.

Product	Unit Size	Cat No.
Cell Meter™ No Wash and Probenecid-Free Endpoint Calcium Assay Kit *Optimized for microplate reader*	100 Tests	36312
Fluo-3, AM *UltraPure grade* *CAS 121714-22-5*	1 mg	21011
Fluo-3, AM *Bulk package* *CAS 121714-22-5*	50 mg	21012
Fluo-3, AM *UltraPure grade* *CAS 121714-22-5*	20x50 mg	21013
Fluo-3, pentasodium salt	1 mg	21016
Fluo-3, pentapotassium salt	1 mg	21017
Fluo-3, pentaammonium salt	1 mg	21018
Fluo-3FF, pentapotassium salt	1 mg	21019
Fluo-4 AM *Ultrapure Grade* *CAS 273221-67-3*	1 mg	20550
Fluo-4 AM *Ultrapure Grade* *CAS 273221-67-3*	10x50 µg	20551
Fluo-4 AM *Ultrapure Grade* *CAS 273221-67-3*	5x50 µg	20552
Fluo-4, Pentapotassium Salt	1 mg	20555
Fluo-4, Pentapotassium Salt	10x50 µg	20556
Screen Quest™ Fluo-4 No Wash Calcium Assay Kit	10 Plates	36325
Screen Quest™ Fluo-4 No Wash Calcium Assay Kit	100 Plates	36326
HHBS [Hanks' Buffer with 20 mM Hepes]	100 mL	20011
Pluronic® F-127 *10% solution in water*	10 mL	20053
ReadiUse™ probenecid *25 mM stabilized aqueous solution*	10x10 mL	20062

NAD+ Integration

In Cellular Pathways

Introduction

The Importance of NAD+ and ROS

The coenzyme nicotinamide adenine dinucleotide (NAD+) is the molecular link between cellular metabolism, signaling, and transcription. Its synthesis, availability, and degradation are therefore central to the function of the cell and in healthy human physiology.

Cellular metabolism is the beginning of all other activities in living cells, providing energy for the millions of biochemical reactions that take place in any given moment. As such, any dysfunction in this process has immediate effects both on an intracellular scale and for overall human health. One of the most heavily studied aspects of this dysfunction is the changing levels and ratios of NAD+ and its related forms and enzymatic cofactors and byproducts.

Reactive Oxygen Species, or ROS, are a potentially damaging biochemical byproduct of multiple cellular pathways that involve redox reactions, with the most prominent contributors being the energy pathways facilitated by the coenzymes NAD+ and NADP. The reduced forms of these coenzymes are used for detoxification of ROS, and the various ROS themselves are used in a temporary fashion for intra- and inter-cellular signaling. There are currently ~400 known redox reactions in the cell that involve NAD+/NADH, and another ~30 for the phosphorylated variation NADP/NADPH. The far-reaching influence of these molecules makes their measurement and visualization useful even in seemingly unrelated experiments.

A phenotype of age is decreased resistance to cellular stress, which can be treated by increased NAD+ levels. The full influence of NAD+ is likely largely unknown and should be explored in multiple experimental fields and contexts. By measuring NAD+ both specifically and in ratio of its oxidized and reduced forms, researchers can discern the many factors at play within both healthy and dysfunctional cell behavior.

Healthy Versus Cancerous Cell Regulation

NAD+ levels and associated enzymes are essential for genomic maintenance. Since genomic stress and damage is the root source of all cancers, NAD+ regulation is of interest in fields that study cancer susceptibility and prevention. Cancer can be simplified as being the condition in which cells forget how to die.

There has been a huge amount of progress and discoveries made in recent years about the protein links between multiple cellular pathways and physiological conditions such as metabolic dysfunction and aging. Better methods of detection and visualization of NAD+ and associated biomolecules are pivotal in gaining further understanding of these interconnected aspects of human health and function.

There is constant crosstalk between the activity of the mitochondria, peroxisomes, and nucleus, which not only is representative of the typical cooperation between the organelles within the cell, but also that of the communication between cell metabolism, regulation, and gene transcription.

There are separate pools of NAD+ used by the cytosol, nucleus, and mitochondria, interconnected by multiple redox processes. Affected cell pathways include glycolysis (occurring within the cytoplasm) and TCA cycle as well as oxidative phosphorylation (within the mitochondria). Although these pathways are location-specific, the cell is able to move NAD+ to the appropriate organelles to a small extent. However, cytoplasmic NAD+ cannot directly cross the mitochondrial membrane, so biosynthesis of NAD+ is of high importance. Compartmentalized NAD+ biosynthesis is also studied in its relationship to cancer cell growth and the deregulation of normal cellular activity.

NAD+ biosynthesis is essential for the energy production of the cell, and the resultant coenzymes are kept in various

locations within the cell. This compartmentalized synthesis is one aspect of the integration of cell transcription, signaling, and metabolism. Increases in cytoplasmic NAD+ reduce nuclear NAD+ levels. Cells require increased cytoplasmic NAD+ to regulate nuclear events during cell differentiation, an example of the close relationship between cell cycle regulation and metabolic activity.

Interconnected Cycles- Chronobiology, Metabolism and Aging Pathologies

Simultaneous Measurement of Related Biomolecules

There are many molecular metabolic regulators, some of which have been studied intensely in recent years as their importance in cellular biology gains more validation. Some of the major molecular families include: peroxisome proliferator activated receptors (PPARs), sirtuins, and multiple kinases, such as AMP-activated protein kinase (AMPK), and protein kinase A (PKA). The interdependent molecular mechanisms that govern cellular metabolism are still being explored, and improved understanding of the overall process requires exploration of their synergistic and additive/subtractive effects of these molecules and their involved pathways on each other.

Consider the well-known sensation of sleepiness after a large meal. This innocuous physiological response is the end result of an intricate biochemical interplay that relates directly to these dinucleotides. Namely, they are the communication between the sleep/wake cycle (circadian clock) and metabolism.

Nocturnin (NOCT) is an enzyme expressed as a factor of the circadian clock. NOCT, potentially along with other proteins, target the mitochondria and dephosphorylate NADP+ and NADPH into their NAD+ and NADH forms, which are immediately accessible to multiple energy-producing pathways. This enzymatic link is one of the most obvious biochemical ties between mammalian circadian rhythm and metabolic activity.

Focusing on a single target or metabolic mechanism can lead to a lack of understanding of the underlying biochemistry and interplay between various pathways that regulate cell behavior and survival. NAD+ has a role in physiological conditions far more dire than after-dinner naps, and measuring its fluctuation is a worthwhile effort regardless of currently-known relations to a particular experiment.

ROS, Enzymatic Activity, and Health

Mitochondrial respiratory chain deficiency has multiple physiological effects, and improving the NAD+/NADH ratio is a promising treatment for at least some of the symptoms.

Intracellular NAD+ levels are significantly lower in diseases associated with aging and metabolic disorders, including mitochondrial dysfunction. NAD+ is critical as an electron carrier for energy production in the cell, as the reversible redox reaction that converts NAD+ to NADH is central for mitochondrial metabolic function and has no NAD+ net loss. There is loss, however, for many cell signaling processes, which use NAD+ as an enzymatic substrate. These include the well-known sirtuin family, which is implicated in metabolic and age-related conditions.

The NAD+/NADH ratio effects SIRT1 enzymatic activity

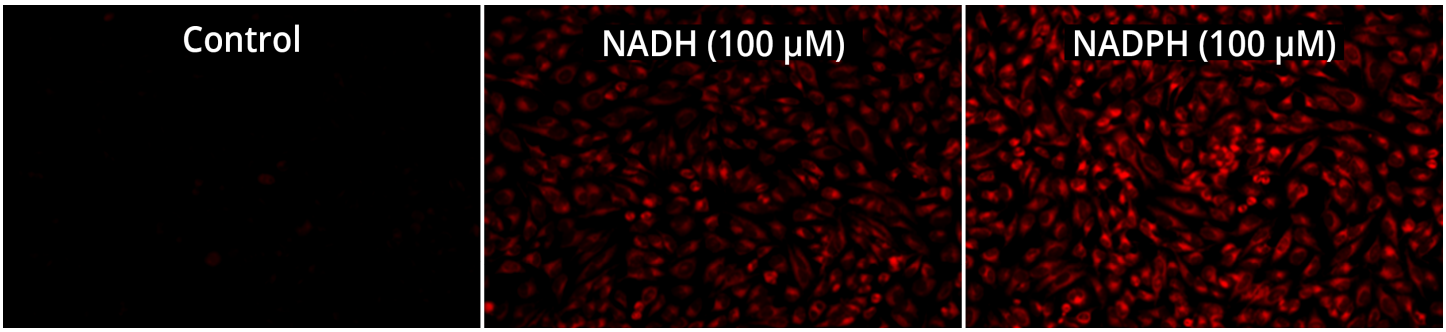

Figure 1. Fluorescence images of NADH/NADPH in HeLa cells using Cell Meter™ Intracellular NADH/NADPH Fluorescence Imaging Kit (Cat No. 15290). HeLa cells were incubated with 100 µM NADH or 100 µM NADPH in serum-free medium for 30 minutes and then co-incubated with JZL1707 NAD(P)H sensor working solution for another 30 minutes. The fluorescence signal was measured using fluorescence microscope with a Cy3® filter.

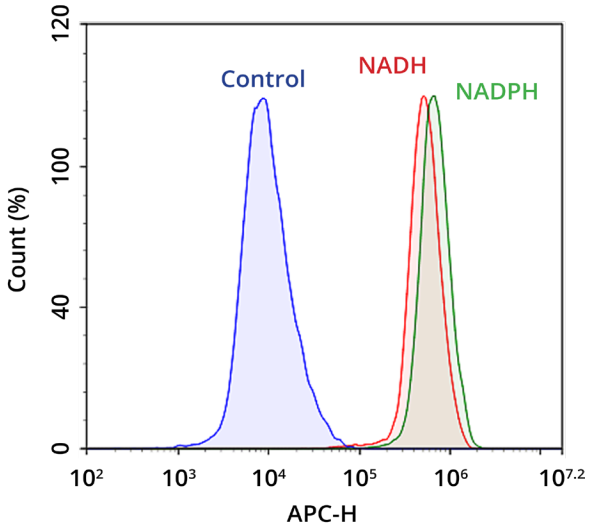

Figure 2. Flow cytometric analysis of NADH/NADPH measurement in Jurkat cells using Cell Meter™ Intracellular NADH/NADPH Flow Cytometric Analysis Kit (Cat No. 15296). Cells were incubated with or without 100 µM NADH in serum-free medium for 30 minutes and then co-incubated with JJ1902 NAD(P)H sensor working solution for another 30 minutes. Fluorescence intensity was measured using ACEA NovoCyte flow cytometer in APC channel.

and the metabolism of adipogenic transcriptional factors. Adipogenesis is regulated by oxidative signaling, so the presence of various ROS within organelles such as peroxisomes or more generally within the cytosol has long-reaching effects. Some types of ROS dysregulation have been shown to have physiological responses with adipose tissue differentiation, leading to dramatic obesity and diabetic symptoms.

Growing Understanding-Methods of Measurements in Living Cells

Intracellular Visualization of NAD(P)+/NAD(P)H

Mitochondrial NAD+ transporters have not yet been identified and isolated in mammals, although they have been in both yeast and bacteria. This is just one of the many aspects of NAD(P)+ movement in the cell that is being explored. Intracellular assays are necessary to measure the changes in nicotinamide levels that indicate the intricate biochemical ballet of the living cell. Outside of the more common cell cycle analyses and similar experiments, there are multiple applications that employ intracellular probes (Figure 1 and 2). NADP+/NADPH ratio can be used to evaluate the redox status of cellular peroxisomes, for example.

The prominence of crosstalk between multiple cellular regulatory pathways has become more apparent in recent years, commensurate with the importance of measuring multiple regulatory factors in bioenergetics experiments.

As diminishing levels of NAD+ are associated with both general age and its attendant pathologies, or in more acute or genetically-caused diseases, there has been increasing interest in therapies that treat these conditions by increasing NAD+ levels within the cell. This intracellular increase is typically attempted by either NAD+ precursor supplements to aid in natural intracellular synthesis, or by inhibiting the enzymes that destructively use NAD+ as a substrate. The benefits observed so far have been in mouse models, and are likely accomplished by the improved accessibility of NAD+ for general cellular metabolic use, for genetic disorders, or alternatively by providing NAD+ sources for the sirtuin enzyme family, of which SIRT1 is one of the most prominently studied.

Living Versus Fixed Cell Protocols and Comparisons

Fixed cells, which have been treated with formaldehyde or similar fixative, are effectively 'stopped' at the moment of fixation, allowing exhaustive examination. This allows exact measurements and detailed answers, but limits the questions that can be answered, given that the cells are dead. Cell lysate is the cytosolic component of lysed cells, separated via centrifuging. The destructive nature of lysate preparation gives limited information about the normal behavior of the cell. In order to improve comprehension of the constantly-changing cellular landscape, living cells are the most difficult and potentially most rewarding subject of study.

Pushing the Envelope-Cell Lysate NAD+/NADH Visualization Techniques

Lysate Isolation Protocols and Uses

In order to produce cell lysate, appropriately chosen cells will be incubated in lysis buffer, which breaks down the outer cell membrane. This controlled destruction is necessary to allow the interior of the cell to be accessed by antibodies (such as

in IHC procedures) and gives consistent results. After the cells have been lysed, they will be centrifuged and the supernatant (containing the collected cytosol of the entire population of treated cells) will typically be selected. Some procedures make use of the organelle pellet instead, which is usually composed of the cell nuclei or mitochondria, for studies targeting cell metabolism.

Using cell lysates provides several advantages for experiments. Multiple sample types (such as tissue or cultures) can be used, including those that have been previously frozen, and they are easy to reproduce. Unfortunately, it is difficult to completely replicate physiological conditions, and pathways such as cell respiration are uncoupled by the lysing procedure. Despite these issues, for experimental questions about enzymatic or catalytic behavior, lysate procedures are often the simplest method to obtain answers.

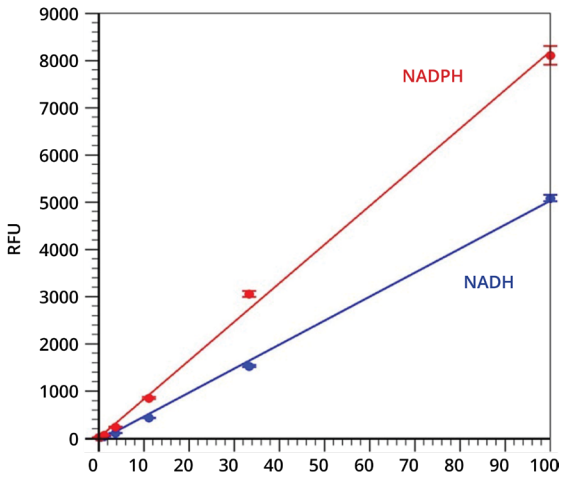

Figure 3. Results of Cell Meter™ Intracellular NADH/NADPH Fluorescence Imaging Kit with Jurkat cell lysate.

Table 1. Detection sensitivity of colorimetric and Fluorimetric Amplite™ NAD(P) and NAD(P)H assay kits.

Product	Assay Target	Detection Limit	Dynamic Range	Catalog No.
Amplite™ Colorimetric NADH Assay Kit	NADH	3 μM	1-200 μM	15271
Amplite™ Colorimetric NADPH Assay Kit	NADPH	3 μM	1-200 μM	15272
Amplite™ Colorimetric NAD/NADH Ratio Assay Kit	NAD/NADH Ratio	0.1 μM	0-3 μM	15273
Amplite™ Colorimetric NADP/NADPH Ratio Assay Kit	NADP/NADPH Ratio	0.03 μM	0.03-1 μM	15274
Amplite™ Colorimetric Total NAD and NADH Assay Kit	NAD+NADH	0.3 μM	0-10 μM	15258
Amplite™ Colorimetric Total NAD and NADH Assay Kit *Enhanced Sensitivity*	NAD+NADH	0.1 μM	0.1-10 μM	15275
Amplite™ Colorimetric Total NADP and NADPH Assay Kit	NADP+NADPH	0.1 μM	0-3 μM	15260
Amplite™ Colorimetric Total NADP and NADPH Assay Kit *Enhanced Sensitivity*	NADP+NADPH	0.03 μM	0.03-1 μM	15276
Amplite™ Fluorimetric Total NAD and NADH Assay Kit *Red Fluorescence*	NAD+NADH	0.1 μM	0-3 μM	15257
Amplite™ Fluorimetric Total NADP and NADPH Assay Kit *Red Fluorescence*	NADP+NADPH	0.01 μM	0-3 μM	15259
Amplite™ Fluorimetric NADH Assay Kit *Red Fluorescence*	NADH	1 μM	0-100 μM	15261
Amplite™ Fluorimetric NADPH Assay Kit *Red Fluorescence*	NADPH	1 μM	0-100 μM	15262
Amplite™ Fluorimetric NAD/NADH Assay Kit *Red Fluorescence*	NAD/NADH Ratio	0.1 μM	0-3 μM	15263
Amplite™ Fluorimetric NADP/NADPH Assay Kit *Red Fluorescence*	NADP/NADPH Ratio	0.01 μM	0-3 μM	15264
Amplite™ Fluorimetric NAD Assay Kit *Blue Fluorescence*	NAD	0.03 μM	0.03-10 μM	15280
Amplite™ Fluorimetric NADP Assay Kit *Blue Fluorescence*	NADP	0.03 μM	0.03-10 μM	15281

Western Blot, Immunoassays and Other Techniques

For immunoprecipitation assays, western blots, and similar procedures, use of cell lysates is standard protocol and gives dependable results. Choosing to employ either colorimetric or fluorimetric detection techniques typically depends on the degree of sensitivity required, the experimental design, and the equipment available. In general, colorimetric tests are simple to run and require more basic laboratory equipment, and fluorimetric assays give more sensitive results.

Conclusion

The edge of science is informed by new information giving rise to new patterns of thought. The paired nicotinamide molecules within the cell still do much that researchers are on the edge of understanding. Employing and improving NAD+ detection in multiple applications will be central to interpreting the interrelated nature of cellular dynamics. NAD+ gains more biological importance with each new discovery and is likely to be a core component of future personalized medical therapies for currently incurable human conditions.

References

1. Poyan Mehr A, Tran MT, Ralto KM, et al. De novo NAD+biosynthetic impairment in acute kidney injury in humans. Nat Med. 2018;24(9):1351"1359.
2. Seo KS, Kim JH, Min KN, et al. KL1333, a Novel NAD+Modulator, Improves Energy Metabolism and Mitochondrial Dysfunction in MELAS Fibroblasts. Front Neurol. 2018;9:552. Published 2018 Jul 5.
3. Pehar M, Harlan BA, Killoy KM, Vargas MR. Nicotinamide Adenine Dinucleotide Metabolism and Neurodegeneration. Antioxid Redox Signal. 2018;28(18):1652"1668.
4. Liu HW, Smith CB, Schmidt MS, et al. Pharmacological bypass of NAD+salvage pathway protects neurons from chemotherapy-induced degeneration. Proc Natl Acad Sci U S A. 2018;115(42):10654"10659.
5. Liu J, Lu W, Shi B, Klein S, Su X. Peroxisomal regulation of redox homeostasis and adipocyte metabolism. Redox Biol. 2019;24:101167.
6. Djouadi F, Bastin J. Mitochondrial Genetic Disorders: Cell Signaling and Pharmacological Therapies. Cells. 2019;8(4):289. Published 2019 Mar 28.
7. Xia M, Zhang Y, Jin K, Lu Z, Zeng Z, Xiong W. Communication between mitochondria and other organelles: a brand-new perspective on mitochondria in cancer. Cell Biosci. 2019;9:27. Published 2019 Mar 19.
8. Estrella MA, Du J, Chen L, et al. The metabolites NADP+and NADPH are the targets of the circadian protein Nocturnin (Curled). Nat Commun. 2019;10(1):2367. Published 2019 May 30.
9. Cantò C, Menzies KJ, Auwerx J. NAD(+) Metabolism and the Control of Energy Homeostasis: A Balancing Act between Mitochondria and the Nucleus. Cell Metab. 2015;22(1):31"53.
10. Ryu KW, Nandu T, Kim J, Challa S, DeBerardinis RJ, Kraus WL. Metabolic regulation of transcription through compartmentalized NAD+Science. 2018;360(6389):eaan5780.

Product	Unit Size	Cat No.
Amplite™ Fluorimetric Glycerol 3-Phosphate (G3P) Assay Kit	200 Tests	13837
Amplite™ Colorimetric Glycerol 3-Phosphate (G3P) Assay Kit	200 Tests	13838
Amplite™ Fluorimetric Total NAD and NADH Assay Kit *Red Fluorescence*	400 Tests	15257
Amplite™ Colorimetric Total NAD and NADH Assay Kit	400 Tests	15258
Amplite™ Fluorimetric Total NADP and NADPH Assay Kit *Red Fluorescence*	400 Tests	15259
Amplite™ Colorimetric Total NADP and NADPH Assay Kit	400 Tests	15260
Amplite™ Fluorimetric NADH Assay Kit *Red Fluorescence*	400 Tests	15261
Amplite™ Fluorimetric NADPH Assay Kit *Red Fluorescence*	400 Tests	15262
Amplite™ Fluorimetric NAD/NADH Ratio Assay Kit *Red Fluorescence*	250 Tests	15263
Amplite™ Fluorimetric NADP/NADPH Ratio Assay Kit *Red Fluorescence*	250 Tests	15264
Amplite™ Colorimetric NADH Assay Kit	400 Tests	15271
Amplite™ Colorimetric NADPH Assay Kit	400 Tests	15272
Amplite™ Colorimetric NAD/NADH Ratio Assay Kit	250 Tests	15273
Amplite™ Colorimetric NADP/NADPH Ratio Assay Kit	250 Tests	15274
Amplite™ Colorimetric Total NAD and NADH Assay Kit *Enhanced Sensitivity*	400 Tests	15275
Amplite™ Colorimetric Total NADP and NADPH Assay Kit	400 Tests	15276
Amplite™ Fluorimetric NAD Assay Kit *Blue Fluorescence*	200 Tests	15280
Amplite™ Fluorimetric NADP Assay Kit *Blue Fluorescence*	200 Tests	15281
Cell Meter™ Intracellular NADH/NADPH Fluorescence Imaging Kit *Red Fluorescence*	100 Tests	15290
Cell Meter™ Intracellular NADH/NADPH Flow Cytometric Analysis Kit *Red Fluorescence*	100 Tests	15291
Cell Meter™ Intracellular NADH/NADPH Fluorescence Imaging Kit *Deep Red Fluorescence*	100 Tests	15295
Cell Meter™ Intracellular NADH/NADPH Flow Cytometric Analysis Kit *Deep Red Fluorescence*	100 Tests	15296

Power Styramide™ Signal Amplification

A Superior Alternative to Tyramide Signal Amplification

Ultra-Sensitive Detection: High-Resolution Imaging of Low-Abundant Targets

Targets of functional importance such as transcription factors, integral membrane proteins and cell-surface cytokine receptors have endogenous expression levels far below the detection capabilities of labeled antibodies. Not only does the abundance of these targets vary by several orders of magnitude, but their spatiotemporal organization within the cell is dynamic making it challenging to visualize. AAT Bioquest's novel Power Styramide™ Signal Amplification (PSA™) system provides an ultra-sensitive method for detecting low-abundance targets in immunocytochemistry (ICC), immunohistochemistry (IHC), and in situ hybridization (ISH) applications. PSA™ imaging technology combines the superior brightness and photostability of iFluor® dyes with HRP"mediated Styramide™ signal amplification to generate fluorscence signals with significantly higher precision and sensitvity, more than 100 times greater than standard ICC/IHC/ISH methods and up to 50 times greater than traditional tyramide signal amplification techniques (Figure 1).

Similar to tyramide signal amplification, PSA™ labeling utilizes an enzyme-mediated detection method that harnesses the catalytic activity of horseradish peroxidase (HRP) to generate high-density labeling of iFluor®dye-Styramide™ conjugates onto a target protein or nucleic acid sequence in situ. In the first step of this process, a probe, such as a primary antibody or nucleic acid sequence, binds to the target via immunoaffinity or hybridization, respectively. This initial complex is then detected with an HRP-labeled secondary antibody or HRP-streptavidin conjugate (if a biotinylated primary antibody was used in the initial detection of the target). Next, multiple copies of a labeled Styramide™, such as iFluor® 488 Styramide™ or iFluor 555™ Styramide™, are activated by enzymatic reaction with HRP. Lastly, the highly reactive, short-lived Styramide™ radicals covalently couple with tyrosine residues proximal to the HRP"target interaction site, resulting in minimal diffusion-related loss of signal localization (Figure 2). Any unbound labeled Styramide™ radicals quickly dimerize, and are washed away to eliminate background.

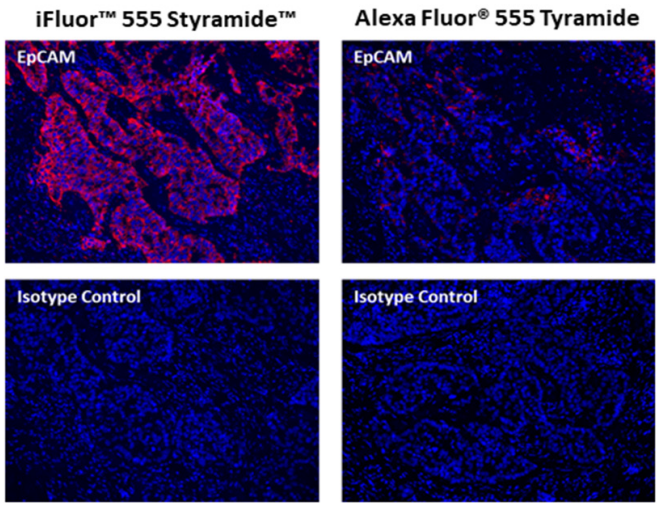

Figure 1. Fluorescence IHC in formaldehyde-fixed paraffin-embedded tissue. Human lung adenocarcinoma sections were incubated with Rabbit mAb EpCAM and its isotype Rabbit IgG control at the same concentration. Tissue sections were then stained with a HRP-labeled Goat anti-Rabbit IgG secondary antibody followed by iFluor® 555 Styramide™ (Left) or Alexa Fluor® 555 tyramide (Right), respectively. Fluorescence images were taken using the TRITC filter set and analyzed with the same exposure time. Data show that Styramide™ super signal amplification can increase the sensitivity of fluorescence IHC over tyramide amplification method. Cell nucleus was stained with Nuclear Blue™ DCS1 (Cat No. 17548).

PSA™ Workflow

1. Fix, permeabilize and block cells or tissue sample. Incubate sample with unlabeled primary antibody, biotinylated primary antibody or biotinylated nucleic acid probe.	2. Add HRP-secondary antibody or HRP-streptavidin conjugate.	3. Add iFluor® dye Styramide™ working solution, allow for HRP-catalyzed deposition of Styramide™	4. Mount sample and detect Signal

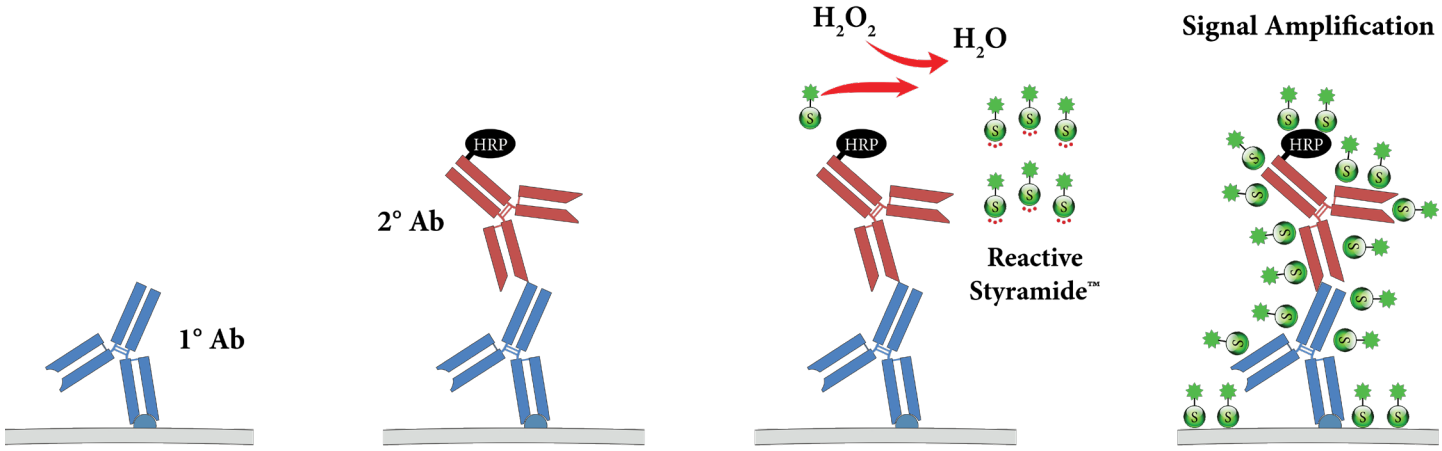

Figure 2. Workflow for Power Styramide™ Signal Amplification (PSA™). With workflow similar to conventional ICC and IHC methods, PSA™ kits and Styramide™ reagents can achieve sensitive detection of desired targets in a few simple steps.

PSA™ Imaging - Greater Sensitivity for Low-Abundance Targets

The Styramide™ signal amplification technique used in our PSA™ Imaging kits utilizes the catalytic activity of HRP for the covalent deposition of labeled Styramide™ proximal to the target of interest. The enhanced sensitivity of the PSA™ Imaging kits over conventional immunofluorescence methods using fluorescently labeled antibodies or other tyramide signal amplification technologies is in part due to improvements in the reagents for each amplification step. Figure 1 shows an example of the improved sensitivity of Styramide™ signal amplification to detect EpCam in human lung adenocarcinoma in comparison to conventional tyramide labeling.

The PSA™ Imaging kits enhance the specific fluorescence signal by utilizing iFluor® dye labeled Styramide™ conjugates, which react with HRP to covalently deposit brightly fluorescent and photostable iFluor® dye Styramides™ on tyrosine residues and other similar molecules in close proximity. Furthermore, Styramide™ radicals have a significantly higher reactivity than traditional tyramide radicals making PSA™ labeling abundantly faster, more robust and sensitive than traditional tyramide signal amplification systems (Figure 3).

PSA™ Imaging kits also employ several strategies to maximize convenience and performance. First, Styramide™ conjugates allow for significantly less consumption of primary antibody compared to coventional immunofluorescence techniques to acheive sensitive detection of low-abundance target molecules. Even with much less primary antibody, PSA™ technology provide detection sensitivities similar to or greater than those obtained using a fluorescently labeled secondary antibody or tyramide signal amplification in an ICC application (Figure 3). Using fewer antibodies per experiment will save on the cost of primary antibodies, a major expense in ICC and

IHC workflows. Also, more experiments can be accomplished using a single vial of primary antibody. Given that some primary antibodies show significant lot-to-lot variation, using a single lot throughout a project can produce more reliable results that are consistent from experiment to experiment. Second, these kits contain highly cross-adsorbed secondary antibodies to help ensure specificity for the target primary antibody with minimal cross-reactivity with other antibody species. For example, HRP"conjugated goat anti"mouse IgG exhibits no detectable reactivity to mouse proteins or IgG derived from other species such as goat, bovine, human, or rat. Lastly, PSA™ Imaging kits include a robust labeling protocol with all the necessary reagents to perform 100 tests.

PSA™ Amplification Is Multiplexable

The PSA™ Imaging kits are available with five spectrally distinct iFluor® dye Styramide™ conjugates and two different

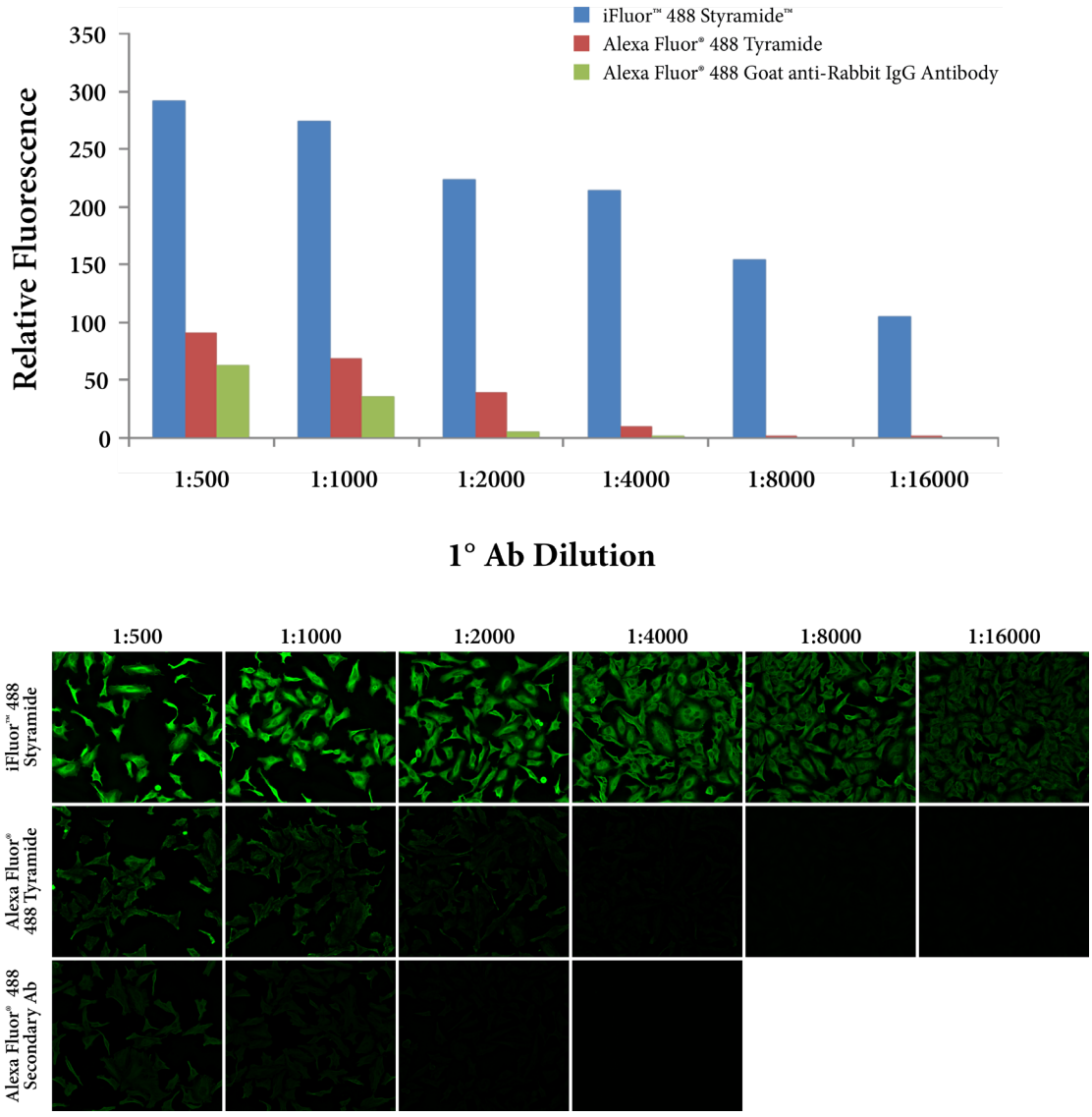

Figure 3. Sensitivity of Power Styramide™ Signal Amplification (PSA™) Kits. HeLa cells were fixed, permeabilized and labeled with various concentrations of rabbit anti-tubulin primary antibody. The manufacturer recommendation was 1:500 dilution or 2 µg/ml. Cells were then stained with reagents in our iFluor® 488 PSA™ Imaging Kit with Goat Anti-Rabbit IgG, an Alexa Fluor® 488-labeled tyramide or an Alexa Fluor® 488-labeled goat anti-rabbit IgG. Cell images were captured from each treatment under the same conditions (using a FITC filter set and analyzed with the same exposure time). Relative fluorescence signal intensity was measured and compared between different detection methods.

HRP secondary reagents (Table 1). Additionally, there are eleven stand-alone iFluor® dye Styramide™ conjugates spanning the UV to NIR for further flexibility in designing multi-parametric applications (Table 2). This range of choices allows high-resolution detection and visualization of multiple signals in a single cell or tissue sample. In addition to multiplex detection using primary antibodies from different species (Figures 4), PSA™ imaging is also compatible with experiments using GFP and RFP fusions as reporters of gene expression.

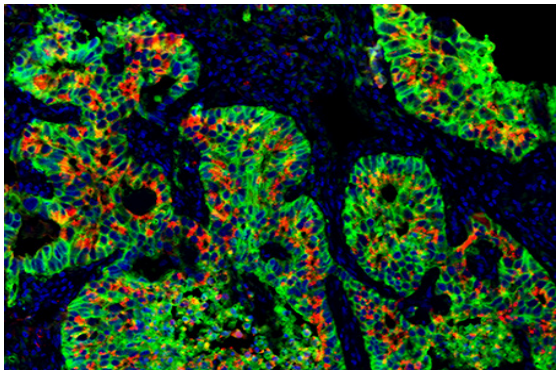

Figure 4. Sequential immunostaining of FFPE human lung adenocarcinoma using two iFluor® PSA™ Imaging kits. EpCam were labeled with rabbit anti-EpCam antibodies and iFluor® 488 PSA™ Imaging Kit with goat anti-rabbit IgG (Cat No. 45205), followed by washing. Pan-Keratin were labeled with mouse anti-pan Keratin antibodies and iFluor® 555 PSA™ Imaging Kit with goat anti-mouse IgG (Cat No. 45270). Nuclei were labeled with DAPI (Cat No. 17513). Images were acquired on a confocal microscope.

Table 1. iFluor® PSA™ Imaging Kits with HRP-secondary antibody conjugates.

Product	Ex (nm)	Em (nm)	Filter Set
iFluor 350™ PSA™ Imaging Kit with Goat Anti-Mouse IgG	344	448	DAPI
iFluor 350™ PSA™ Imaging Kit with Goat Anti-Rabbit IgG	344	448	DAPI
iFluor 488™ PSA™ Imaging Kit with Goat Anti-Mouse IgG	491	514	FITC
iFluor 488™ PSA™ Imaging Kit with Goat Anti-Rabbit IgG	491	514	FITC
iFluor 555™ PSA™ Imaging Kit with Goat Anti-Mouse IgG	552	567	Cy3/TRITC
iFluor 555™ PSA™ Imaging Kit with Goat Anti-Rabbit IgG	552	567	Cy3/TRITC
iFluor 594™ PSA™ Imaging Kit with Goat Anti-Mouse IgG	592	619	Cy3/TRITC
iFluor 594™ PSA™ Imaging Kit with Goat Anti-Rabbit IgG	592	619	Cy3/TRITC
iFluor 647™ PSA™ Imaging Kit with Goat Anti-Mouse IgG	649	665	Cy5
iFluor 647™ PSA™ Imaging Kit with Goat Anti-Rabbit IgG	649	665	Cy5

Table 2. iFluor® Styramide™ Reagents For iFluor® Secondary Reagents.

Product	Ext. Coeff.1	FQY2	Ex (nm)	Em (nm)	Filter Set
iFluor® 350 Styramide *Superior Replacement for Alexa Fluor 350 tyramide*	20,000	0.95	345	442	DAPI
iFluor® 488 Styramide *Superior Replacement for Alexa Fluor 488 tyramide*	75,000	0.9	491	514	FITC
iFluor® 546 Styramide *Superior Replacement for Alexa Fluor 546 tyramide*	100,000	0.67	541	557	Cy3/TRITC
iFluor® 555 Styramide *Superior Replacement for Alexa Fluor 555 tyramide*	100,000	0.64	552	567	Cy3/TRITC
iFluor® 568 Styramide *Superior Replacement for Alexa Fluor 568 tyramide*	100,000	0.57	568	587	Cy3/TRITC
iFluor® 594 Styramide *Superior Replacement for Alexa Fluor 594 tyramide*	180,000	0.53	587	603	Cy3/TRITC
iFluor® 647 Styramide *Superior Replacement for Alexa Fluor 647 tyramide*	250,000	0.25	654	669	Cy5
iFluor® 680 Styramide *Superior Replacement for Alexa Fluor 680 tyramide*	220,000	0.23	683	700	Cy5
iFluor® 700 Styramide *Superior Replacement for Alexa Fluor 700 tyramide*	220,000	0.23	690	713	Cy7
iFluor® 750 Styramide *Superior Replacement for Alexa Fluor 750 tyramide*	270,000	0.12	759	777	Cy7
iFluor® 790 Styramide *Superior Replacement for Alexa Fluor 790 tyramide*	250,000	0.13	786	811	Cy7

Product	Unit Size	Cat No.
iFluor 350™ PSA™ Imaging Kit with Goat Anti-Rabbit IgG	100 Tests	45200
iFluor 350™ PSA™ Imaging Kit with Goat Anti-Mouse IgG	100 Tests	45250
iFluor 488™ PSA™ Imaging Kit with Goat Anti-Rabbit IgG	100 Tests	45205
iFluor 488™ PSA™ Imaging Kit with Goat Anti-Mouse IgG	100 Tests	45260
iFluor 555™ PSA™ Imaging Kit with Goat Anti-Rabbit IgG	100 Tests	45220
iFluor 555™ PSA™ Imaging Kit with Goat Anti-Mouse IgG	100 Tests	45270
iFluor 594™ PSA™ Imaging Kit with Goat Anti-Rabbit IgG	100 Tests	45230
iFluor 594™ PSA™ Imaging Kit with Goat Anti-Mouse IgG	100 Tests	45280
iFluor 647™ PSA™ Imaging Kit with Goat Anti-Rabbit IgG	100 Tests	45240
iFluor 647™ PSA™ Imaging Kit with Goat Anti-Mouse IgG	100 Tests	45290
iFluor® 350 Styramide *Superior Replacement for Alexa Fluor 350 tyramide*	100 Slides	45000
iFluor® 488 Styramide *Superior Replacement for Alexa Fluor 488 tyramide*	100 Slides	45020
iFluor® 546 Styramide *Superior Replacement for Alexa Fluor 546 tyramide*	100 Slides	45025
iFluor® 555 Styramide *Superior Replacement for Alexa Fluor 555 tyramide*	100 Slides	45027
iFluor® 568 Styramide *Superior Replacement for Alexa Fluor 568 tyramide*	100 Slides	45030
iFluor® 594 Styramide *Superior Replacement for Alexa Fluor 594 tyramide*	100 Slides	45035
iFluor® 647 Styramide *Superior Replacement for Alexa Fluor 647 tyramide*	100 Slides	45045
iFluor® 680 Styramide *Superior Replacement for Alexa Fluor 680 tyramide*	100 Slides	45050
iFluor® 700 Styramide *Superior Replacement for Alexa Fluor 700 tyramide*	100 Slides	45055
iFluor® 750 Styramide *Superior Replacement for Alexa Fluor 750 tyramide*	100 Slides	45065
iFluor® 790 Styramide *Superior Replacement for Alexa Fluor 790 tyramide*	100 Slides	45070

Fluorescent Detection of Cell Senescence

For Flow Cytometry and Imaging Applications

Beta Galactosidase Assay - Senescence Assay Using Fluorescence Substrate

Cellular senescence is a state of stable growth arrest, and is thought to play a physiological role in normal development and tissue homeostasis. It is characterized by morphological and metabolic alterations, altered gene expression and upregulation of pro-inflammatory secretomes. It plays a physiological role in normal development and tissue homeostasis. There are several factors that drive senescence in cells, including telomere damage in senescence caused by ageing and metabolic dysfunction. Since many pathways are associated with this process, senescence can be detected by looking into genotypic changes. Genotypic changes are sometimes cell-specific and the intensity of the activating response varies. Evidence suggests that senescence-associated β-gal activity is highly upregulated and can be used to detect senescent cells. This assay is particularly useful for screening novel drug candidates that intitate senescence in cells or conditions that cause genotypic changes leading to senescence. In this AssayWise letter, we will discuss data from our cell senescence probe Xite™ β-D-galactopyranoside and its detection of senescent cells.

The identification of senescent cells is based on an increased level of lysosomal β-galactosidase (SA-β gal) activity. The first method to detect senescence-associated SA-β gal activity includes a cytochemical protocol that is suitable for the histochemical detection of individual senescent cells in culture and tissue biopsies. Cells under normal growth conditions produce SA-β gal, which is located in lysosomes. This enzymatic activity can be detected at pH 4.0 using the chromogenic substrate 5-bromo 4 -chloro3-indolyl β-D-galactosidase (X-gal). The SA-β gal positive cells can be scored under bright-field microscopy. Cytochemical methods can take approximately 30 to 60 minutes to execute and several hours to a day to develop and record the response. The disadvantage of using this method is lack of sensitivity and quantitation.

The second method is based on the use of 5-dodecanoylaminofluorescein di-β-D-galactopyranoside (C12FDG), a fluorogenic substrate for β-galactosidase. This compound is membrane-permeable and nonfluorescent before hydrolysis; after hydrolysis of the galactosyl residues by β-galactosidase, the compound emits green fluorescence upon excitation and remains confined within the cell. The C12-FDG provides better sensitivity than the cytochemical method but it is still not up to standard. We recently released a new probe which addresses the issue of low sensitivity of the C12-FDG probe for fluorescence analysis and is very easy to use. Xite™ β-D-galactopyranoside detects the SA-β gal at almost 10 times lower concentrations with better cell permeability then C12-FDG. Xite™ β-D-galactopyranoside contains a fluorophore attached to galactosyl moieties and lacks fluorescence. However, in the presence of β-gal enzyme, the galactosyl group gets cleaved, separating the galactosyl residue from the fluorophore and thus provides fluorescence. This meticulous mechanism of the probe and lack of fluorescence in the absence of β-gal enzyme provides better specificity towards β-gal enzyme in the cells.

Materials and Methods

Cell Culture and Reagents

Jurkat cells were maintained in RPMI-1640 medium containing 10% Fetal Bovine Serum (FBS). HeLa cells were

maintained in Dulbecco's Modified Eagle Medium (DMEM) containing 10% FBS. Reaction Buffer was used from Cat No. 23005, AAT Bioquest, Inc. Camptothecin and β-Galactosidase enzyme were purchased from Sigma and used as per manufacturer's recommendations.

Ex/Em Measurement in the Presence and Absence of Enzyme

In 2 mL of PBS, 100 uL of Xite™ β-D-galactopyranoside stock solution (2 μM) was added in reaction buffer without and with β-gal enzyme (2 U/mL) and Ex/Em was measured using Varian Eclipse® fluorescence spectrophotometer.

Flow Cytometry Analysis

To induce senescence, Jurkat cells were treated with Camptothecin at 5 μM final concentration and incubated at 37C incubator for 6 hours. Cells were washed with DPBS and then stained with 5 μM probe constituted in reaction buffer for 30 minutes at 37C incubator. Cells were then washed twice with DPBS and resuspended in Reaction Buffer. Flow cytometry was performed with FITC channel using NovoCyte® flow cytometer from ACEA Biosciences.

Acquisition of Fluorescence Images

HeLa cells were treated in a black 96-well plate and stained as indicated earlier. Fluorescence images were acquired using FITC filter set on fluorescence microscope.

Fluorescence Plate Reader Analysis

Different doses of β-galactosidase enzyme was incubated alongside FDG or Xite™ β-D-galactopyranoside at the same concentration in a black wall clear bottom 96-well plate and fluorescence was measured using a Spectramax GeminiXS® (Molecular Devices) fluorescence plate reader at Ex/Em= 490/525 nm with the cutoff 515 nm.

Results

Ex/Em in the Presence and Absence of Target Enzyme

In order to verify the specificity of our Xite™ β-D-galactopyranoside, we measured excitation and emission in the presence and absence of β-gal enzyme. As we hypothesized that the Xite™ β-D-galactopyranoside only emits fluorescence in the presence of its respective enzyme, a significant amount of fluorescence was only observed upon presence of β-gal enzyme. This further strengthens the selectivity towards research studies that are conducted to differentiate senescent cells.

Detection of Drug-Induced Senescence Inside Cells Using Flow Cytometry and Fluorescence Imaging

Next, we shifted our testing to cells expressing higher concentrations of SA-β-gal enzyme with drug-induced senescence. We treated Jurkat cells with Campothecin to induce

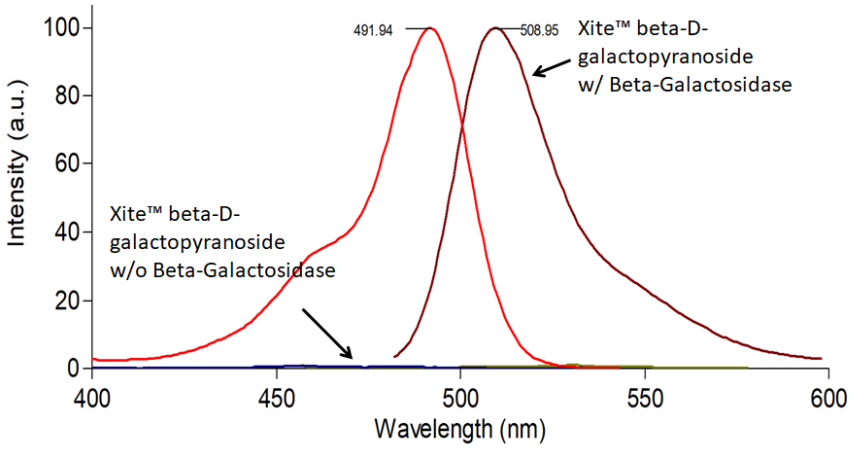

Figure 1. Ex/Em spectrum of Xite™ β-D-galactopyranoside in the absence and presence of β-galactosidase.

senescence, followed by incubation with either our Xite™ β-D-galactopyranoside or FDG. Samples were processed through flow cytometry (Figure. 2A) or fluorescence microscopy (Figure. 2B). The flow cytometry analysis showed that the Xite™ β-D-galactopyranoside gave almost 10-fold higher fluorescence intensity in camptothecin-treated cells compared to the untreated samples. Unlike our Xite™ β-D-galactopyranoside, the FDG did not produce any significant fluorescence with treated samples, mainly due to lack of cell permeability. This comparison sheds more light on how effectively our Xite™ β-D-galactopyranoside could be used for drug analysis in cell senescence studies.

Response Comparison Between FDG and Xite™ β-D-Galactopyranoside Using Fluorescence Microplate Reader

Earlier we speculated that the response with FDG was lower because of the lack of cell permeability. To explore this possibility, we investigated the sensitivity of our Xite™ β-D-galactopyranoside for the detection of β-gal enzyme and compared the results with FDG. We ran the assay with different concentrations of β-gal enzyme and treated with 1 µM of either our Xite™ β-D-galactopyranoside or FDG and recorded the response using the fluorescence plate reader. A 10-fold higher response was obsereved with Xite™ β-D-galactopyranoside compared to FDG, which cements our notion that Xite™ β-D-galactopyranoside has a higher efficiency and signal intensity over other commercially available probes.

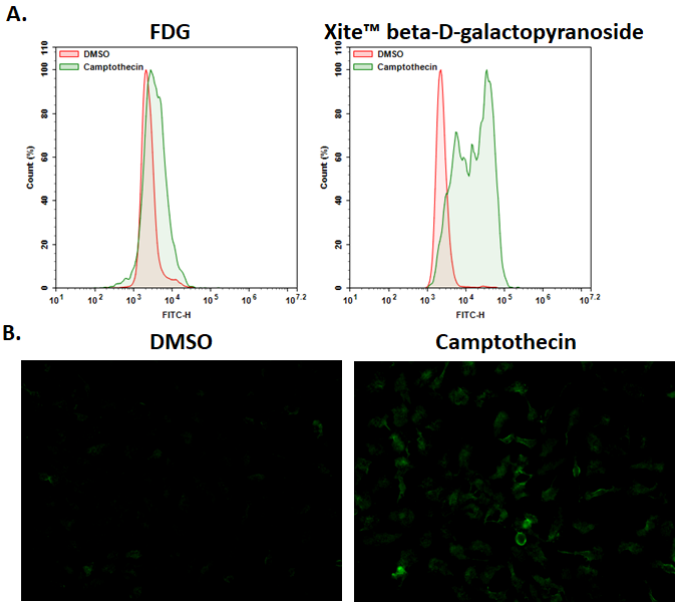

Figure 2. Drug-induced senescence was detected with Xite™ β-D-galactopyranoside using flow cytometry (A) and fluorescence microscopy (B).

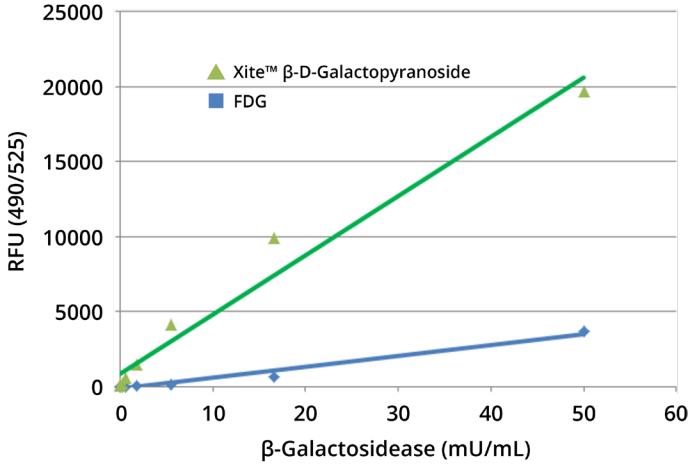

Figure 3. Comparison between Xite™ beta-D-galactopyranoside and FDG with Beta-galactosidase enzyme using a fluorescence microplate reader.

References

1. McHugh, D., & Gil, J. (2018). Senescence and aging: Causes, consequences, and therapeutic avenues. The Journal of cell biology, 217(1), 65"77. doi:10.1083/jcb.201708092
2. Debacq-Chainiaux, J. D. Erusalimsky, J. Campisi, O. Toussaint, Protocols to detect senescence-associated beta-galactosidase (SA-βgal) activity, a biomarker of senescent cells in culture and in vivo, Nat. Protoc. 2009, 4, 1798.
3. Lòpez-Otin C, Blasco MA, Partridge L, Serrano M, Kroemer G. The hallmarks of aging. Cell. 2013;153(6):1194"1217.
4. Itahana K, Campisi J, Dimri GP. (2007). Methods to detect biomarkers of cellular senescence: the senescence-associated beta-galactosidase assay. Methods Mol Biol 371: 21"31.

Product	Unit Size	Cat No.
Xite™ Green beta-D-galactopyranoside	1 mg	14030
Xite™ Red beta-D-galactopyranoside	1 mg	14035
Cell Meter™ Cellular Senescence Activity Assay Kit *Green Fluorescence*	100 Tests	23005
Cell Meter™ Cellular Senescence Activity Assay Kit *Red Fluorescence*	100 Tests	23007

Previous Issue

AssayWise Letter Volume 8 Issue 1

Featured Articles

Introducing CytoCite™ Fluorometer with Cloud-Integration

ReadiView™ Biotin: All-In-One Biotinylation & Quantification of Biotin Labeling

Fundamentals of Flow Cytometry

ReadiUse™ Lyophilized Phycobiliproteins

Buccutite™ Fluorescent Protein and Tandem Dye Antibody Labeling Kits

AAT Bioquest, Inc.

5775 W Las Positas Blvd
Pleasanton, CA 94588
United States
Tel: +1 800 990 8053
Fax: +1 800 609 2943
Email: support@aatbio.com

For Research Use Only. Not for use in diagnostic or therapeutic procedures.

SILVER
ecovadis
Sustainability Rating

aatbio.com/resources/assaywise

International Distributors

Australia:
Assay Matrix Pty Ltd.
Email: info@assaymatrix.com
Website: http://www.assaymatrix.com/

Jomar Life Research
Email: info@JLresearch.com.au
Website: https://jlresearch.com.au/

Austria:
Biomol GmbH
Email: info@biomol.de
Website: https://www.biomol.de/

Belgium:
Bio-Connect B.V.
Email: info@bio-connect.nl
Website: https://www.bio-connect.nl/

Gentaur BVBA
Email: info@gentaur.com
Website: https://gentaur.com/

Canada:
Cedarlane Laboratories Ltd.
Email: sales@cedarlanelabs.com
Website: http://www.cedarlanelabs.com/

China:
AmyJet Scientific
Email: sales@amyjet.com
Website: https://www.amyjet.com/

Biolite Biotech Co., Ltd
Email: info@tjbiolite.com
Website: https://www.xabiolite.cn/

Dakewe Biotech
Email: bj_info@dakewe.net
Website: http://www.bio-city.net/

Croatia:
Biomol GmbH
Email: info@biomol.de
Website: https://www.biomol.com/

Czech Republic:
EXBIO Praha, a.s.
Email: info@exbio.cz
Website: https://www.exbio.cz/

Scintila, s.r.o.
Email: rejtharkova@scintila.cz
Website: http://www.scintila.cz

Denmark:
Nordic BioSite ApS
Email: info@nordicbiosite.dk
Website: http://www.nordicbiosite.dk

Estonia:
Biomol GmbH
Email: info@biomol.de
Website: http://www.biomol.de

Nordic BioSite AB
Email: info@biosite.se
Website: http://www.biosite.se

Finland:
Nordic BioSite OY
Email: info@biosite.fi
Website: http://www.biosite.fi

France:
CliniSciences
Email: info@clinisciences.com
Website: https://www.clinisciences.com/en/

EUROMEDEX
Email: research@euromedex.com
Website: http://www.euromedex.com

Interchim
Email: interchim@interchim.com
Website: http://www.interchim.com

Ozyme
Email: tech@ozyme.fr
Website: https://yris.ozyme.fr/en

Germany:
Biomol GmbH
Email: info@biomol.de
Website: http://www.biomol.de

Hungary:
Biomol GmbH
Email: info@biomol.com
Website: https://www.biomol.com/

IZINTA Trading Co., Ltd.
Email: baloghk@izinta.hu
Website: http://www.izinta.hu

Iceland:
Nordic BioSite AB
Email: info@biosite.se
Website: http://www.biosite.se

India:
Everon Life Sciences
Email: info@everonlife.com
Website: http://www.everonlife.com/

GenxBio Health Sciences Pvt. Ltd,
Email: sales@genxbio.com
Email: genxbio@gmail.com
Website: http://www.genxbio.com

KRISHGEN BioSystems
Email: info@krishgen.com
Website: https://www.krishgen.com/

Ireland:
Generon
Email: info@generon.ie
Website: https://www.generon.ie/

Stratech Scientific Ltd.
Email: info@stratech.co.uk
Website: http://www.stratech.co.uk

Israel:
ADVANSYS Technologies for Life Ltd.
Email: info@advansys.co.il
Website: http://www.advansys.co.il

Israel:
Doron Scientific
Email: info@doronscientific.com
Website: https://www.doronscientific.com/

Italy:
DBA Italia s.r.l.
Email: info@dbaitalia.it
Website: https://www.dbaitalia.it/

Japan:
Cosmo Bio Co., Ltd.
Email: mail@cosmobio.co.jp
Website: http://www.cosmobio.co.jp

Nacalai Tesque, Inc.
Email: info@nacalaiusa.com
Website: http://www.nacalai.com

Latvia and Lithuania:
Nordic BioSite AB
Email: info@biosite.se
Website: http://www.biosite.se

Lebanon:
DPC-Lebanon sarl
Email: sales2@dpcleb.com
Website: https://www.dpcleb.com/

Malaysia:
Mbioscience Solutions Sdn Bhd
Email: info@mbioscience.com
Website: http://www.mbioscience.com/

Mexico:
CIDSA Mexico
Email: ventas@cidsamexico.com
Website: https://www.cidsamexico.com/

Morocco:
HexaBiogen
Email: maroc@hexabiogen.com
Website: https://www.hexabiogen.com/

Netherlands:
ITK Diagnostics BV
Email: info@itk.nl
Website: http://www.itk.nl

New Zealand:
Scienze Ltd
Email: info@scienze.nz
Website: https://scienze.nz/

Norway:
Nordic BioSite AB
Email: info@biosite.se
Website: http://www.biosite.se

Poland:
Biomol GmbH
Email: info@biomol.de
Website: http://www.biomol.de

Gentaur Sp. z. o. o.
Email: poland@gentaur.com
Website: https://www.gentaur.pl/

International Distributors

Portugal:
Abyntek Biopharma S.L.
Email: info@abyntek.com
Website: http://www.abyntek.com/

Deltaclon
Email: info@deltaclon.com
Website: https://www.deltaclon.com/

Romania:
SC VitroBioChem SRL
Email: office@vitro.ro
Website: http://www.vitro.ro

Serbia:
Biologist Group d.o.o.
Email: office@biologist.rs
Website: http://www.biologist.rs/

Singapore and Other South Asian Countries:
Axil Scientific Pte Ltd
Email: info@axilscientific.com
Website: https://www.axilscientific.com/

ProBioscience Technologies Pte Ltd
Email: info@probioscience.org
Website: https://www.probioscience.org/

Slovakia:
Scintila, s.r.o.
Email: rejtharkova@scintila.cz
Website: https://www.scintila.cz/

South Korea:
Cheong Myung Science Corporation
Email: cms@cmscorp.co.kr
Website: http://www.cmscorp.co.kr

EdithGen
Email: edithgen@daum.net
Website: http://www.edithgen.com/

Kimnfriends Corporation
Email: kimnfriends@hanmail.net
Website: http://www.kimnfriends.co.kr

Sungwoo LifeScience
Email: sungwoo_ls@hanmail.net
Website: http://www.sungwools.com/

Spain:
Abyntek Biopharma S. L.
Email: info@abyntek.com
Website: https://www.abyntek.com/

Deltaclon S. L
Email: info@deltaclon.com
Website: http://www.deltaclon.com

Sweden:
Nordic BioSite AB
Email: info@biosite.se
Website: http://www.biosite.se

Switzerland:
LuBioScience GmbH
Email: info@lubio.ch
Website: http://www.lubio.ch

Taiwan:
Rainbow Biotechnology Co., LTD.
Email: rainbow@rainbowbiotech.com.tw
Website: http://www.rainbowbiotech.com.tw

Thailand:
Pacific Science Co., Ltd.
Email: order@pacificscience.co.th
Website: https://www.pacificscience.co.th/

Turkey:
Suarge Biyoteknoloji Ltd. Co.
Email: info@suarge.com
Website: http://suarge.com/

United Kingdom:
Stratech Scientific Ltd.
Email: info@stratech.co.uk
Website: http://www.stratech.co.uk

Vietnam:
Truong Bio, Inc.
Email: info@truong.bio
Website: https://www.truong.bio/

Online Marketplaces & Services

United States:
Avantor/VWR
Email: technicalproductSupportNA@vwr.com
Website: https://us.vwr.com/store/

Fisher Scientific:
Tel: 1-(800)-766-7000
Website: http://www.fishersci.com/

Intramalls
Email: info@intramalls.com
Website: https://intramalls.com/

United States:
Quartzy
Email: support@quartzy.com
Website: https://www.quartzy.com/

Science Exchange
Email: info@scienceexchange.com
Website: https://www.scienceexchange.com/

Scientist
Email: support@scientist.com
Website: https://www.scientist.com/

United States:
Zageno
Email: support@zageno.com
Website: https://zageno.com/

AAT Bioquest®

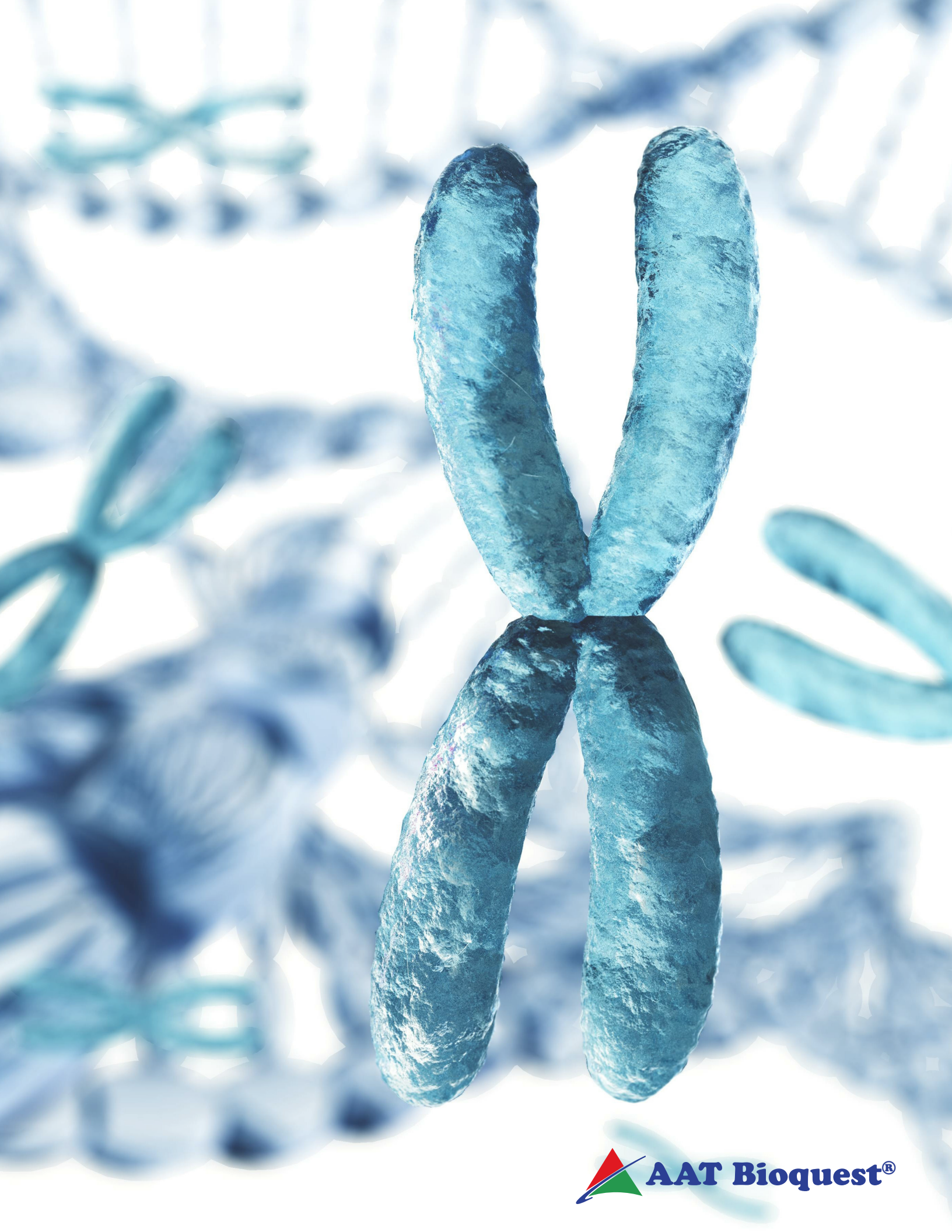
AAT Bioquest®